Economic Geology
Vol. 95, 2000, pp. 1445–1472

Porphyry Gold Deposits of the Refugio District, Maricunga Belt, Northern Chile

JOHN L. MUNTEAN[†,*] AND MARCO T. EINAUDI

Department of Geological and Environmental Sciences, Stanford University, Stanford, California 94305-2115

Abstract

The porphyry gold deposits of the Refugio district and similar deposits in the Maricunga belt contain the lowest known copper to gold ratios (% Cu/ppm Au = ~0.03) of any porphyry-type deposit. The gold deposits are associated with subvolcanic andesitic to dacitic intrusions emplaced into coeval volcanic rocks. Both the Verde and Pancho deposits are zoned in space from a deeper zone of banded quartz veinlets associated with chlorite-magnetite-albite and/or pyrite-albite-clay alteration to a shallow zone of pyrite-albite-clay and local quartz-alunite ledges. Pancho contains an additional, deepest, porphyry copperlike zone, with quartz veinlets (A-veinlets) and potassic alteration. Relative to Verde, Pancho is telescoped, with all three zones present within a 400-m-vertical interval.

The porphyry copperlike zone at Pancho is characterized by A-veinlets and pervasive potassic alteration, both restricted to intrusive rocks. A-veinlets range from hairline streaks of magnetite ± biotite with minor quartz and chalcopyrite, and K feldspar alteration envelopes to sugary quartz veinlets <1 cm in width with magnetite and chalcopyrite and no alteration envelopes. Hypersaline liquid inclusions coexisting with vapor-rich inclusions indicate temperatures above 600°C and salinities as high as 84 wt percent NaCl equiv. A pressure estimate of 250 bars indicates a depth of 1,000 m, assuming lithostatic pressure. Potassic alteration consists of a central zone of magnetite-K feldspar-oligoclase that changes outward to a biotite-rich zone. Total sulfide content, predominately as chalcopyrite, is generally <1 vol percent, whereas magnetite content is 2 to 5 percent. Where A-veinlets and potassic alteration predominate, grades are typically 0.1 wt percent hypogene copper and 0.5 to 1 ppm gold.

Banded quartz veinlets are present at both Verde and Pancho, where they occur mostly above A-veinlets and cut A-veinlets where they overlap. They are less than 2 cm in thickness and lack alteration envelopes. Dark gray bands, whose color is due to abundant vapor-rich fluid inclusions and micrometer-sized grains of magnetite, commonly occur as symmetric pairs near the vein walls. The bands are commonly botryoidal and are continuous through quartz grains, suggesting that the quartz recrystallized from a silica gel. Rare liquid-rich fluid inclusions in quartz indicate temperatures ≤350°C and salinities <35 wt percent NaCl equiv. Estimated pressures are <200 bars, suggesting depths of 190 to 1,500 m under hydrostatic pressure. Gold occurs both in the dark bands with magnetite and outside the dark bands with pyrite, chlorite, illite, and K feldspar. Banded veinlets occupy steeply dipping radial and shallowly dipping concentric fractures. Zones of abundant banded veinlets without early A-veinlets generally contain 0.5 to 2 ppm gold and <0.05 wt percent hypogene copper.

Most of the differences between porphyry gold deposits at Refugio and porphyry copper deposits can be attributed to shallower depths of formation—less than 1 km compared to 1.5 to 4 km that is typical for porphyry copper deposits. Shallower depths resulted in lower sulfide concentrations, local garnet veinlets, widespread albite-bearing alteration, and most importantly banded quartz veinlets, which are unique to porphyry gold deposits. Banded quartz veinlets are a direct result of episodic intrusion of magma to within 1 km of the surface and exposure of high-temperature magmatic fluids to hydrostatic pressures. Episodic rupturing of a brittle-ductile boundary surrounding the intrusive centers at Verde and Pancho led to flashing of magmatic fluids, loss of sulfur to vapor, and low sulfide/gold ratios in ore.

Introduction

OVER the past several decades, field studies of porphyry copper deposits (e.g., papers in Titley, 1966; Gustafson and Hunt, 1975; Dilles and Einaudi, 1992) have led to summaries of their common features (e.g., Lowell and Guilbert, 1970; Sillitoe, 1973; Titley and Beane, 1981), but surprisingly few papers have focused on their differences (Kesler, 1973; Gustafson, 1978; Sillitoe, 1979, 1993). The 1990s have seen several additions of new subtypes to the class of porphyry-type deposits, including the porphyry gold deposits of the Maricunga belt, Chile (Vila and Sillitoe, 1991). For this reason it is becoming increasingly important to identify factors that control the variations among members of this class. The porphyry gold deposits at Refugio in the Maricunga belt contain the lowest known copper:gold ratios of any porphyry-type deposit, and previous studies have established their similarities to gold-rich porphyry copper deposits (Vila and Sillitoe, 1991; Vila et al., 1991). One of the orebodies at Refugio, Pancho, does share many characteristics of porphyry copper deposits. However, the most copper-poor gold orebody at Refugio, Verde, lacks many of the features that are commonly used to classify deposits as porphyry copper deposits.

In this paper we describe the geology, wall-rock alteration, vein styles, and fluid inclusions at Refugio and contrast these features with those of porphyry copper deposits. Important differences include paleodepths of less than a kilometer (rather than 1.5–4 km that is typical for porphyry copper deposits, cf. Sillitoe, 1973), spatial association of gold ore with chlorite-magnetite-albite alteration (rather than with potassic), and the presence of gold within banded quartz-magnetite

[†] Corresponding author: e-mail, JLMuntean@aol.com
[*]Present Address: Placer Dome Exploration Inc., 240 S. Rock Blvd., Suite 117, Reno, Nevada 89502.

veinlets that have not been described from porphyry copper deposits. These veinlets, in part recrystallized from silica gel, contain a fluid inclusion assemblage, which suggests that saline hydrothermal fluids flashed within the vapor + salt field in the system water-NaCl at high temperatures (~600°C) and low pressures (100–200 bars).

Geology of the Maricunga Belt

The Maricunga belt is a region of numerous gold-silver-copper prospects and deposits in the high Andes of northern Chile (Vila and Sillitoe, 1991; Fig. 1). Zones of hydrothermally altered rocks give rise to strong color anomalies detectable by satellite imagery and aerial photography (Fig. 2). The color anomalies result mainly from weathering of pyritic zones in argillized rocks. Several of the altered zones host significant metal concentrations, including high-sulfidation epithermal gold-(silver) deposits (La Coipa, La Pepa) and porphyry gold-(copper) deposits (Refugio, Aldebaran, Marte, Lobo). Since 1980, an aggregate geologic resource of approximately 40 Moz of gold has been defined.

The Maricunga belt occupies a north-northeast-trending chain of andesitic to dacitic volcanoes that are part of a late Oligocene to late Miocene continental margin volcanic-plutonic arc. The geology of the belt (Fig. 2) has been defined by the regional studies of Segerstrom (1968), Zentilli (1974),

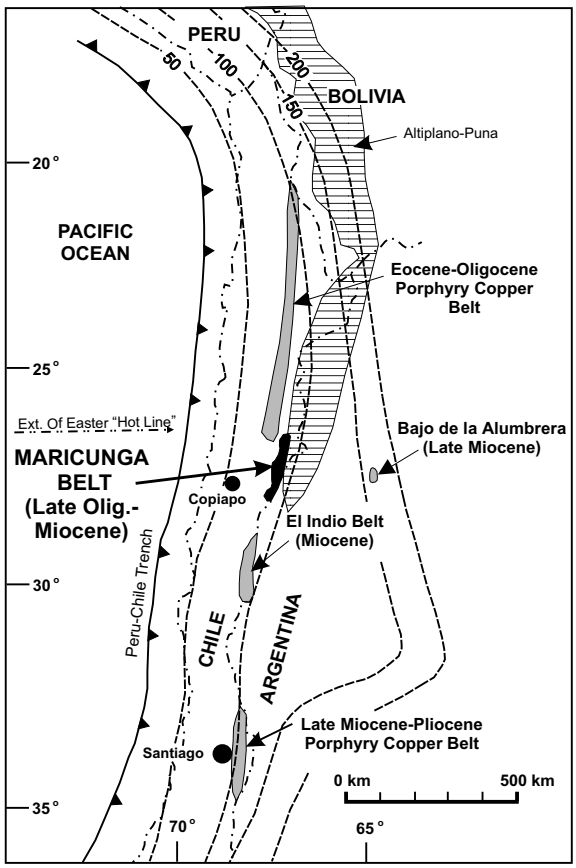

FIG. 1. Map showing the location of the Maricunga belt relative to other regional zones of important copper-gold mineralization in Chile and Argentina. Also shown are the Altiplano-Puna and the extension of the Easter hot line. The contour lines represent depths in kilometers to the Benioff zone. Modified from Davidson and Mpodozis (1991).

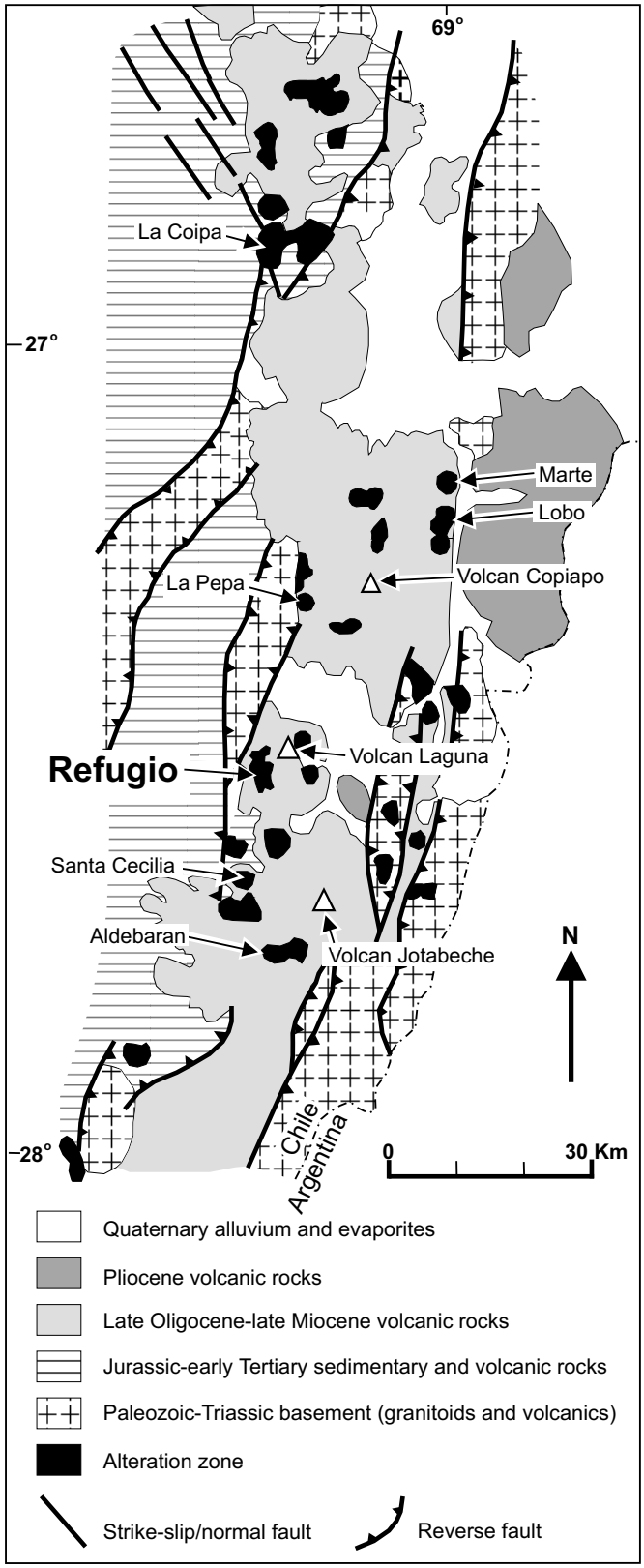

FIG. 2. Schematic geologic map of the Maricunga belt. Modified from Davidson and Mpodozis (1991).

Mercado (1982), Davidson and Mpodozis (1991), and Mpodozis et al. (1995). Paleozoic-Triassic basement rocks crop out in north-northeast-trending horst blocks. Four main episodes of mostly andesitic to dacitic arc magmatism occurred in the Maricunga belt from the late Oligocene to the early Pliocene (Kay et al., 1994; Mpodozis et al., 1995). The first (26–20 Ma, late Oligocene to early Miocene) and second (16–11 Ma, middle Miocene) episodes resulted in numerous stratovolcanic complexes and dome fields along the length of the belt. Igneous rocks genetically linked to gold ores in the Refugio district are part of the first episode. The third (11–7 Ma, late Miocene) and fourth (7–5 Ma, late Miocene to earliest Pliocene) episodes are represented by dacitic volcanic rocks at Volcán Copiapó and Volcán Jotabeche, respectively (Fig. 2).

The Maricunga belt lies near the northern boundary of the modern nonvolcanic, flat-slab region of the Chilean Andes (28–33° S, Fig. 1). Flattening of the subduction zone began around 20 to 17 Ma (Jordan et al., 1983; Isacks, 1988; Allmendinger et al., 1990; Kay et al., 1991), after termination of the first magmatic episode and prior to initiation of the second. The Maricunga belt lies in a transition zone where there is a gradual decrease in the dip of the Nazca plate from 30° to 10° as lat 28° S is approached from the north (Barazangi and Isacks, 1976; Bevis and Isacks, 1984). Shallowing of the subducting slab may have been responsible for the eastward shift in magmatic activity in the Pliocene (Walker et al., 1991; Kay et al., 1994).

Three main structural trends are present in the Maricunga belt. First, north to northeast-trending high-angle reverse faults that bound basement rocks (Fig. 2) are probably coincident with the onset of flattening of the subduction zone (Davidson and Mpodozis, 1991; Vila and Sillitoe, 1991; Kay et al., 1994; Mpodozis et al, 1995). A second structural trend consists of northwest-striking normal faults, dikes, and veins, suggesting southwest-northeast extension (Oviedo et al., 1991; Vila and Sillitoe, 1991; Vila et al., 1991; King, 1992). These structures are found in many of the late Oligocene to early Miocene volcanic centers (Mpodozis et al., 1995). A third structural trend is defined by east-northeast satellite lineaments interpreted by King (1992) as dextral shear zones that mark the southern boundary of the Altiplano-Puna plateau. The lineaments are coincident with the on-land projection of the Miocene to Recent submarine volcanic chain off the Chilean coast (Bonatti et al., 1977), east-west patterns in aeromagnetic data (King, 1992), and the boundary between two basement domains, the Arequipa-Antofalla craton to the north and the Chilenia and Precordillera terranes to the south (Ramos et al., 1986; Tosdal, 1996). These coincidences suggest a crustal discontinuity that may have been a primary regional control on the magmatism and metallogeny of the Maricunga belt (cf. Sasso and Clark, 1998).

Background of Exploration and Development at Refugio

In 1984 Compania Minera Refugio registered claims at Refugio and identified three areas anomalous in gold, named Verde, Pancho, and Guanaco (Brown and Rayment, 1991; Sillitoe, 1995; Fig. 3). Between 1985 and 1987, Minera Anglo American, under option, defined about 9 million tons (Mt) of oxidized material with an average grade of 0.93 g/t gold at Verde but decided to terminate its option (Sillitoe, 1995).

In 1989 Bema Gold (Chile) Limitada, in joint venture with Compania Minera Refugio, outlined a large volume of oxidized gold ore underneath postore cover to the east of Verde (Verde East in Fig. 3). By 1991, drilling had established a mineable reserve at Verde of 101 Mt of 1.02 g/t gold at a cutoff of 0.5 g/t (Brown and Rayment, 1991). The average copper grade at Verde is 0.03 percent (Flores, 1993) for both oxidized and unoxidized ores. Bema also outlined a geologic resource at Pancho of 81 Mt of 0.85 g/t gold (Flores, 1993). Drill hole assays at Pancho indicate hypogene copper grades between 0.05 and 0.2 percent. In 1993, Bema established a 50:50 joint venture agreement with Amax Gold Inc. Mining at Verde commenced in late 1995 with a 30,000 t/d open-pit, heap-leaching operation.

Methods Employed

Eight km of road cuts were mapped at the Verde and Pancho deposits at scales of 1:1,000 or greater and surrounding areas were mapped at a scale of 1:10,000. Ten Verde core holes (1,150 m) and four Pancho core holes (250 m) were logged. A color-coded mapping and logging scheme similar to that used by the Anaconda Company in the 1960s was employed, which includes graphical and numerical data on rock type, structure, vein types, relative ages of intrusions and vein types, mineral associations, and approximate volume percent of minerals and veins. Original volume percent of sulfide in weathered samples was estimated from the abundance of indigenous limonite and leached cavities. Sawed surfaces of nearly 500 samples were examined by binocular microscope, and 180 polished thin sections were studied by reflected and transmitted light microscope. In addition to 5,000 2-m channel samples assayed by Anglo-American, 161 channel samples of intervals mapped during this study were assayed for gold. X-ray diffraction, X-ray fluorescence, and electron microprobe analyses were used to document chemical composition of rocks and minerals. Fluid inclusions from 14 doubly polished plates were described and microthermometric data were collected from five samples.

District Geology

Porphyry gold deposits are hosted by the Refugio volcanics (Fig. 3) of late Oligocene to early Miocene age (22–24 Ma, Sillitoe et al., 1991; Mpodozis et al., 1995; Muntean, 1998). The Refugio volcanics, an informal term, are covered in the eastern portion of the district by mid-Miocene volcanic rocks whose source was La Laguna stratovolcano located about 6 km to the east (McKee et al., 1994). Basement rocks of Paleozoic to early Tertiary age are exposed in the western part of the district (Fig. 3). These include Late Pennsylvanian to Triassic rhyolitic pyroclastic rocks, lifted up along a northeast-trending reverse fault and forming most of the high ridge west of Refugio. Late Jurassic to early Tertiary red beds, propylitized andesite flows, and andesitic volcaniclastic rocks with an aggregate thickness of 1,100 m crop out in the southwestern part of the district.

The Refugio volcanics, exposed over at least 12 km^2, consist of andesitic-dacitic flows and breccias and dacite porphyry domes, intruded by subvolcanic quartz diorite porphyry stocks and breccia pipes. The total thickness of the Refugio volcanics is approximately 700 m in the center of the district.

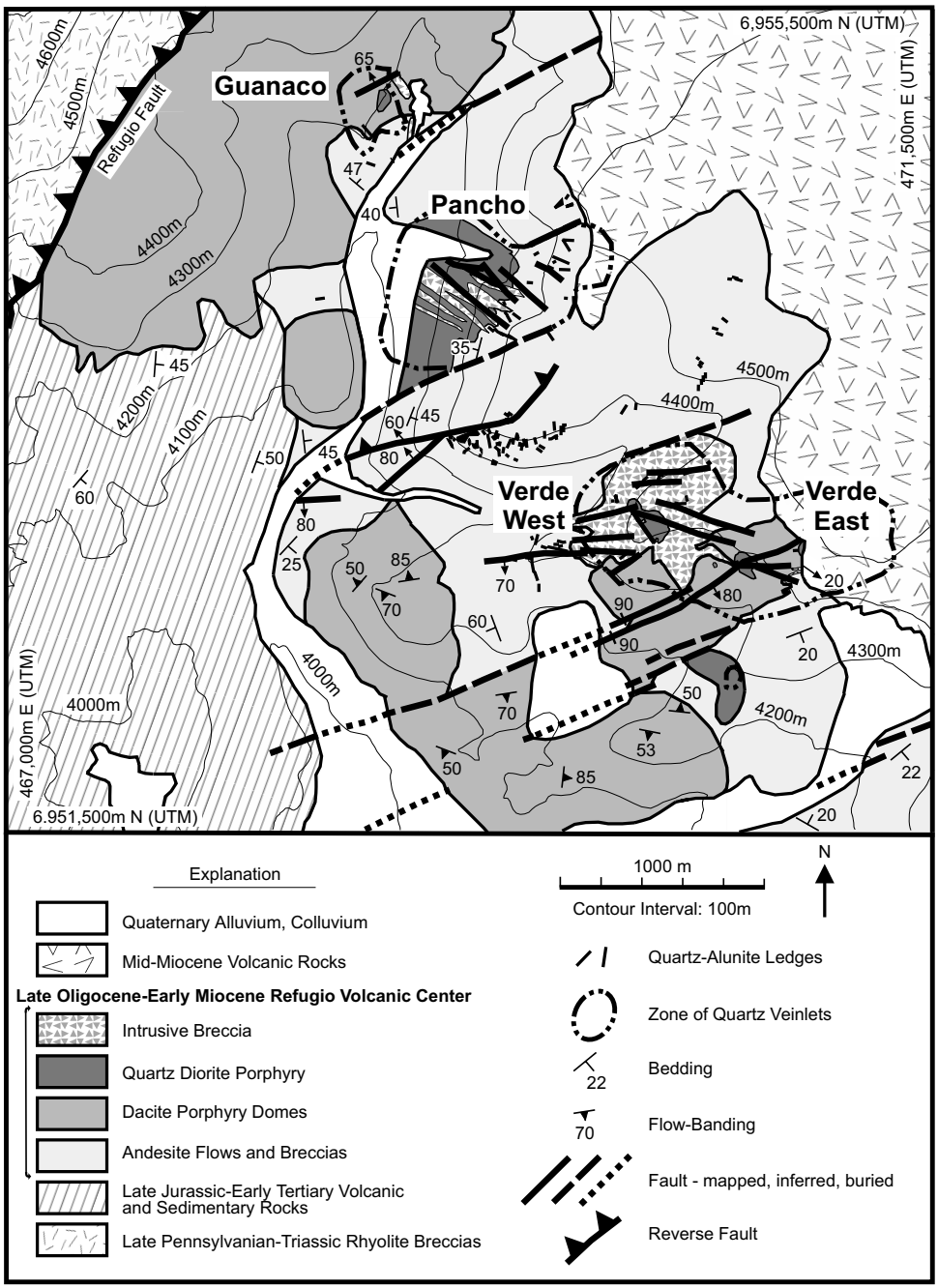

FIG. 3. Map of the district geology at Refugio, based on the present study.

Although the rocks in the volcanic center can be readily classified as either porphyries or breccias based on texture, subclassification within these two categories (Tables 1 and 2) is difficult, especially in areas of hydrothermal alteration. Porphyritic lava flows, domes, and subvolcanic intrusions have similar phenocryst assemblages of plagioclase + hornblende + biotite + magnetite-ilmenite ± quartz ± augite. Therefore, map units are distinguished by their groundmass characteristics, outcrop appearance (Table 2), and contact relationships. Compositions of the least altered and least weathered igneous rocks are listed in Table 3.

Andesite flows and breccias

Rocks shown as andesite flows and breccias in Figure 3 include monolithic breccias, heterolithic breccias, and porphyritic flows of andesitic to dacitic composition. Monolithic breccias are interpreted as either block and ash deposits or autobrecciated flow margins related to the extrusion of dacite porphyry domes. Heterolithic breccias are more widespread than monolithic breccias and are interpreted as lahars or pyroclastic flow deposits. Porphyritic andesite, present as layered lava flows, occurs in a discontinuous, arcuate band along

TABLE 1. Breccias of the Refugio Volcanic Center

Type	Outcrop appearance	Description of fragments	Matrix
Volcanic, monolithic (block and ash deposit-autobrecciated flow margin?)	Massive, locally layered	Matrix-supported, subangular, mostly lapilli sized (up to meters) lithic fragments of dacite porphyry (50–75%); broken phenocrysts	Clastic, mostly <15 μm
Volcanic, heterolithic (lahar?-pyroclastic flow?)	Massive, locally layered	Matrix-supported, lapilli-sized, subangular lithic fragments of dacite porphyry and quartz diorite porphyry; possible altered pumice (15–25%); broken phenocrysts (up to 50%)	Clastic, mostly <25 μm
Intrusive	Heterogeneous, massive, steep intrusive contacts with other units, irregular and dikelike forms	Matrix-supported, lapilli-sized, well-defined fragments of immediate wall rock and poorly defined porphyritic autoliths (5–60%); broken phenocrysts; An_{37} to An_{44}	Uneven, anhedral granular or interlocking, mostly <100 μm; commonly hydrothermally altered; altered rock flour(?) and/or igneous(?); resorbed quartz phenocrysts

TABLE 2. Porphyritic Rocks of the Refugio Volcanic Center

Map unit (Fig. 3)	Outcrop appearance	Phenocrysts[1]	Groundmass
Andesite flows	Mostly layered lava flows	Plagioclase: 35%,≤6 mm, mostly 0.5–1.5 mm; oscillatory zoning, An_{41} to An_{64}; hornblende: 9%, ≤5 mm, mostly 0.5–2 mm; biotite: 1%, ≤2 mm; magnetite-ilmenite: 3%, ≤1.2mm, mostly <0.25 mm; augite: local, <2%; trace zircon, apatite	50–55%, mostly <5 μm; dull, aphanitic, brownish in transparent light; anhedral quartz and K-rich alkali feldspar, subhedral plagioclase; probably devitrified
Dacite porphyry domes	Flow banded or massive; local intrusive contacts with volcanic rocks	Plagioclase: 40%, ≤7 mm, mostly 0.5–2 mm, oscillatory zoning, An_{37} to An_{56}; hornblende: 7%, ≤8 mm, mostly 0.5–3 mm; biotite: 2.5%, ≤6 mm, mostly 1–3 mm; quartz: 2%, ≤6 mm, mostly <1 mm, commonly rounded and resorbed; magnetite-ilmenite: 2.5%, ≤1 mm, mostly <0.25 mm; augite: local, <4%, <0.5 mm; trace zircon, apatite	45–50%, mostly <20 μm; cryptocrystalline to microcrystalline, locally turbid; anhedral quartz and K-rich alkali feldspar, subhedral plagioclase (An_{10}– An_{45}), chlorite
Quartz diorite porphyry	Massive; local flow banding; steep intrusive contacts with other units	Plagioclase: 40%, ≤8 mm, mostly 1–2 mm, oscillatory zoning, An_{38} to An_{54}; hornblende: 7%, ≤12 mm, mostly 1–3 mm, commonly poikilitic with plagioclase and magnetite-ilmenite inclusions; biotite: 2.5%, ≤12 mm, mostly 0.5–3 mm; quartz: 0.5%, ≤2 mm, mostly <1 mm, commonly rounded and resorbed; magnetite-ilmenite: 2.5%, ≤1 mm, mostly <0.25 mm; trace zircon, apatite, sphene	45–50%, mostly 10–40 μm; microaplitic, transparent; sugary under a hand lens; anhedral quartz and K-rich alkali feldspar(Or_{71}–Or_{96}), subhedral plagioclase (An_9–An_{54}), chlorite

[1] Percentages are averages of visual estimates of volume percent in thin sections and cut slabs; grain sizes refer to long dimensions; the anorthite and orthoclase components of feldspars are based on electron microprobe analyses that are described and listed in Muntean (1998)

the southern and western edges of the district with a true thickness up to 350 m. The groundmass is aphanitic in hand sample and is brown and cryptocrystalline under uncrossed polars in thin section. The groundmass is interpreted to have been originally glassy.

The sequence of porphyritic andesite flows and breccias that crop out southeast of Verde East dip fairly consistently 20° southeast. Projection of these rocks northwestward suggests the removal of at least 400 to 500 m of rock above the Verde deposit. Westward projection of andesite breccias overlying the east end of Pancho requires the removal of at least 400 m of rock above the lower exposed parts of the Pancho deposit (Fig. 3).

Dacite porphyry

Flow-banded dacite porphyry domes with autobrecciated margins crop out extensively along the southern and western edges of Verde, whereas massive dacite porphyry, which is mainly intrusive in nature, occurs at Verde and Guanaco (Fig. 3). The groundmass of the dacite porphyry is cryptocrystalline to microcrystalline, locally turbid, and is mostly <20 μm in grain size.

Quartz diorite porphyry

Gold is most closely associated in time and space with small stocks of quartz diorite porphyry and intrusive breccia that are distinctly aligned along a northwest trend (Fig. 3). Where

TABLE 3. Whole-Rock Chemical Analyses of Igneous Rocks

Sample no.	RV045	RV078	RV069	DD-1 92-94m[1]	RV050	RR005	RG002	RP050	DD-33 12-14m[1]	DD-24 32-34m[1]	RR017	RR021	RV001	RV037	RP043	RV034
Field name/ map unit	Mid-Miocene Volcanics	Quartz diorite porphyry	Quartz diorite porphyry	Quartz diorite porphyry	Quartz diorite porphyry	Quartz diorite porphyry	Quartz diorite porphyry	Quartz diorite porphyry	Intrusive breccia	Intrusive breccia	Dacite porphyry	Dacite porphyry	Dacite porphyry	Dacite porphyry	Andesite flow	Andesite flow
Oxides (wt %)																
SiO_2	60.2	61.1	59.9	60.9	59.2	60.3	60.3	61.8	63.9	63.0	59.3	60.3	60.1	58.6	59.4	58.5
Al_2O_3	17.1	16.9	17.1	16.4	17.0	16.6	16.9	17.6	14.5	15.0	16.6	16.7	16.0	16.0	17.0	17.1
CaO	5.80	5.02	5.11	3.95	5.73	4.44	4.70	2.96	1.75	5.53	5.63	5.61	3.90	4.69	4.93	5.61
MgO	1.74	1.98	1.90	1.93	2.07	2.14	2.17	1.51	2.95	1.97	2.07	2.09	2.95	2.43	2.24	2.47
Na_2O	3.95	3.64	3.68	3.92	3.49	3.88	3.62	3.96	3.93	3.20	3.71	3.59	3.12	3.36	3.16	3.23
K_2O	2.17	2.18	2.06	2.13	1.96	2.14	2.21	2.07	2.17	1.56	2.04	2.13	2.40	2.16	2.09	2.03
Fe_2O_3[2]	4.76	4.64	5.13	5.37	5.24	5.14	4.72	4.65	5.24	4.96	5.08	4.97	4.95	5.71	5.81	6.26
MnO	0.09	0.17	0.12	0.23	0.13	0.22	0.16	0.12	0.19	0.13	0.09	0.10	0.19	0.21	0.20	0.11
TiO_2	0.690	0.591	0.626	0.610	0.646	0.592	0.598	0.558	0.519	0.579	0.657	0.630	0.562	0.591	0.649	0.681
P_2O_5	0.26	0.22	0.23	0.23	0.24	0.22	0.23	0.08	0.16	0.24	0.23	0.22	0.20	0.21	0.21	0.22
Cr_2O_3	<0.01	<0.01	<0.01	<0.01	<0.01	<0.01	<0.01	<0.01	<0.01	<0.01	<0.01	<0.01	<0.01	<0.01	<0.01	<0.01
LOI	1.65	1.50	2.40	2.40	2.25	2.45	2.45	3.00	3.00	0.95	1.80	2.05	4.10	4.40	2.50	2.45
Sum[3]	98.6	98.1	98.4	98.2	98.1	98.3	98.2	98.5	98.4	97.3	97.4	98.6	98.6	98.5	98.4	98.8
Trace elements (ppm)																
Rb	74	86	60	72	67	68	71	59	84	72	98	63	65	76	54	68
Sr	709	597	591	559	581	587	591	489	427	568	680	538	424	508	537	585
Y	17	26	17	22	23	24	23	20	21	27	39	17	17	23	24	23
Zr	162	161	149	152	156	148	161	153	123	141	161	152	139	142	138	143
Nb	10	9	8	10	11	9	10	7	6	10	13	8	8	8	9	9
Ba	717	692	634	631	672	819	706	698	518	514	694	640	721	732	746	581

Samples were analyzed by X-ray fluorescence by XRAL Laboratories, Toronto, Canada; samples are weakly weathered and/or weakly propylitically altered; sample descriptions and locations are in Muntean (1998)

[1] Depth in meters below drill collar

[2] All iron reported as Fe_2O_3

[3] Low sums probably resulted from incomplete loss on ignition, especially from sulfates

exposed, contacts of quartz diorite porphyry and intrusive breccia indicate that these rocks intruded massive dacite porphyry, andesite flows and breccias, and each other. Quartz diorite porphyry occurs as subequant bodies that range in diameter from 500 m at Pancho to 100 to 200 m at Guanaco and Verde. Under a hand lens the groundmass can be seen as distinctly sucrose, in contrast with the aphanitic groundmass of dacite porphyry and porphyritic andesite. In thin section, the groundmass is microaplitic with a 10- to 40-μm grain size.

Intrusive breccia

Breccia bodies range from irregular, multiple-phase bodies up to 800 m across to dikes centimeters to meters in width. They generally contain 5 to 60 percent lapilli-sized, matrix-supported fragments, including well-defined subangular fragments of the immediate wall rock and autoliths set in a very fine grained matrix (Fig. 4). Autoliths have indistinct boundaries, and their groundmass and phenocryst assemblages are similar to that of quartz diorite porphyry. The breccia matrix has a sandy texture at the scale of a hand sample, commonly showing fine-scale layering that suggests fluidization (Fig. 4A). Except for the broken crystals, the matrix lacks definitive clastic textures or textures, suggesting precipitation of minerals in open space. Where the matrix has a granular texture, it appears to have crystallized from a melt. Where the matrix has an interlocking texture, it may have resulted from hydrothermal alteration of igneous matrix. Numerous samples show fragments of breccia within breccia (Fig. 4B, C), indicating episodic emplacement. Similar mineralogy and the close spatial relationship between intrusive breccia and quartz diorite porphyry suggest a genetic link between the two. The intrusive breccias may have resulted from explosive volatile release and fragmentation of the parent magma of quartz diorite porphyry.

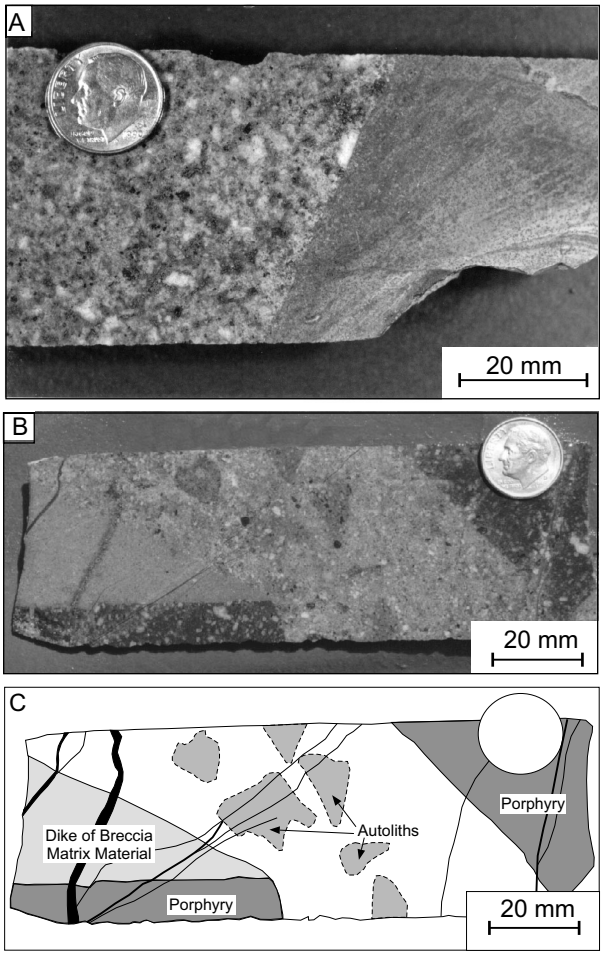

FIG. 4. A. Core sample showing dike from Verde West consisting of fine-grained breccia matrix material. Note the fine-flow layering in dike. B, C. Core sample of intrusive breccia from Verde West. Note the porphyry cut by intrusive breccia matrix material at the left side of the sample and the poorly defined autoliths in the center of the sample. The porphyry and dike were subsequently fragmented, incorporated into intrusive breccia, and cut by banded quartz veinlets.

Structural geology

Refugio is located on the western edge of a graben bounded by a high-angle reverse fault, referred to here as the Refugio fault. The Refugio fault strikes N 20° to 35° E, and places Late Pennsylvanian to Triassic rhyolite in contact with Mesozoic red beds and greenstones. It also juxtaposes these basement rocks with dacite porphyry of the Refugio volcanics (Fig. 3). Thus, final movement on the Refugio fault postdated emplacement of the Refugio volcanics and its associated gold deposits.

Quartz diorite porphyry stocks, intrusive breccia bodies, zones of quartz veinlets, and gold deposits are distinctly aligned along a N 30° to 45° W trend (Fig. 3). Further, dikes of intrusive breccia commonly strike northwest, and some of the quartz diorite porphyry bodies are elongated northwest-southeast. Faults locally strike northwest, but their strike lengths are mostly less than a few hundred meters and displacement on them is less than a few meters. Quartz-alunite ledges occupy northwest-trending faults at Pancho, suggesting these faults were active during hydrothermal activity

Verde Gold Deposit

Gold ore at Verde is associated with a zone of quartz veinlets trending N 80° W that is about 1,500 m long and 600 m wide (Fig. 3). The Verde deposit is composed of two separate coalescing annular-shaped orebodies referred to as Verde West and Verde East. The orebodies have diameters of about 500 m, low-grade cores with diameters of about 100 to 150 m, and vertical extents of more than 500 m.

Geology of the Verde orebodies

Gold mineralization at Verde is hosted by a composite intrusive center consisting of massive dacite porphyry emplaced before mineralization, intrusive breccia bodies emplaced during mineralization, and small stocks of quartz diorite porphyry emplaced during the final stages of mineralization. The main host rock at Verde West is a body of intrusive breccia, 800 m in diameter, with contacts dipping within 10° of vertical (Figs. 3 and 5). The breccia body cuts dacite porphyry and volcaniclastic breccias of the andesite flow and breccia unit. Quartz veinlets hosted by intrusive breccia and dacite porphyry are commonly truncated at steep contacts with late quartz diorite porphyry. Vein abundance in the quartz diorite porphyry at Verde West decreases from 2.5 vol percent along its margins

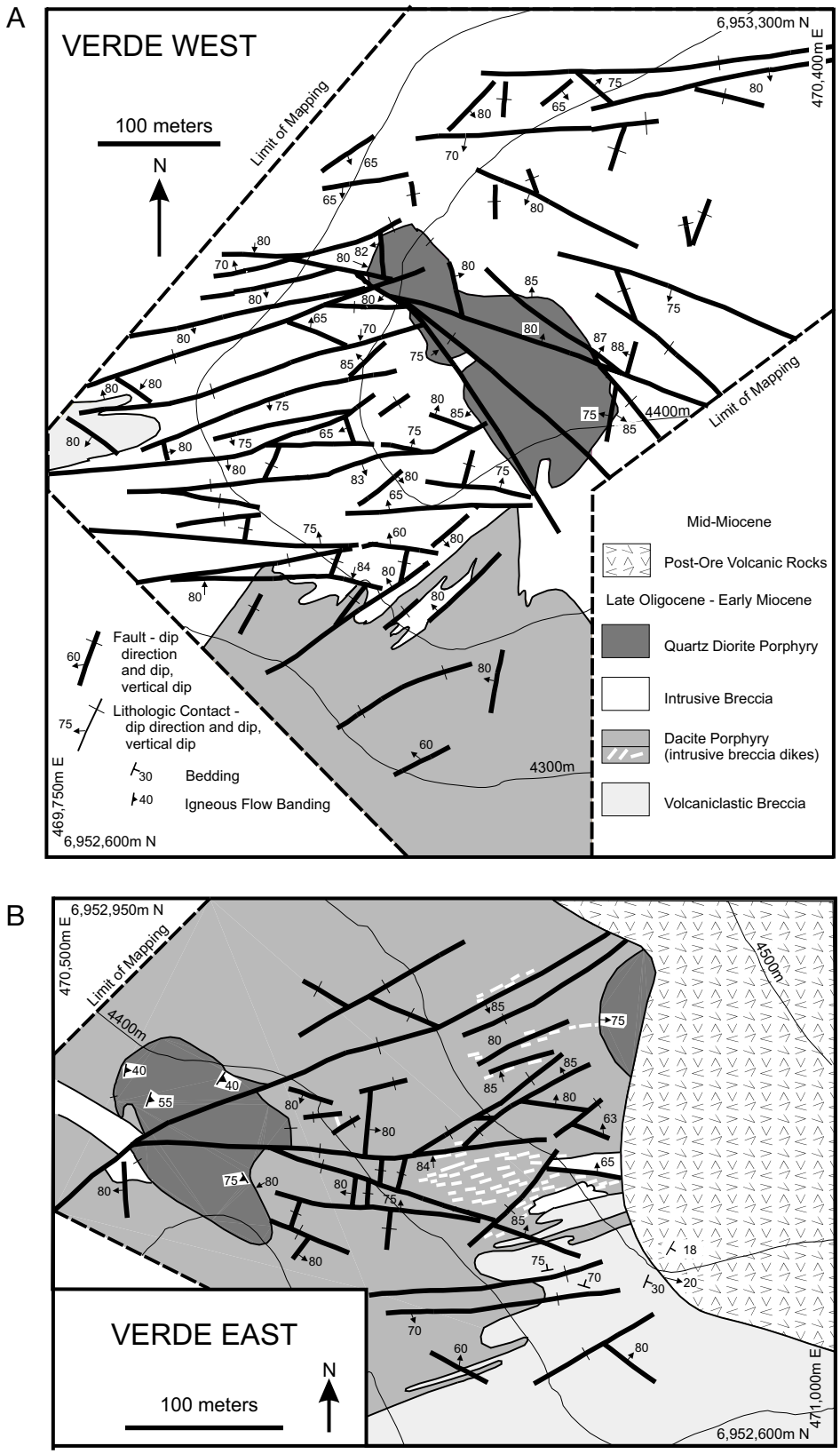

FIG. 5. Geologic maps of the Verde orebodies, based on the present study. A. Verde West, not including unexposed southeastern portion. B. Southwestern exposed portion of Verde East.

to mostly less than 0.25 percent in its interior. Quartz diorite porphyry in the center of the Verde East orebody contains no quartz veinlets.

The Verde orebodies are cut by numerous faults with steep dips. The primary trend strikes N 60° to 90° E; there is a secondary trend striking N 50° to 85° W and a tertiary trend striking N 10° E. Faults commonly occur at contacts between intrusive phases, truncate quartz veinlets, and have fragments of quartz veinlets in clay-rich gouge. Faults do not abruptly terminate or offset ore zones or alteration patterns, suggesting only small postore displacement.

Near-perfect patterns of radial quartz veinlets with high-angle dips and concentric quartz veinlets with low-angle inward dips are present at both Verde West and Verde East (Fig. 6). The patterns are centered on the late stocks of quartz diorite porphyry in the center of the orebodies. Concentric veinlets, analogous to cone sheets, are mostly found between elevations of 4,325 and 4,400 m at Verde West. Mutual cross-cutting relationships between radial and concentric veinlets indicate they are coeval. An additional set of quartz veinlets strikes N 70° E at Verde East, parallel to a fault zone.

Most hydrothermal alteration at Verde and Pancho was pervasive and affected large volumes of rock. Alteration minerals rarely can be tied to individual fractures or veinlets. On a district scale, weak propylitic alteration affected all of the Refugio volcanics and the late quartz diorite porphyry stocks at Verde. Mafic mineral phenocrysts are partially replaced by chlorite and magnetite, but their cleavage outlines are retained. Deposit-specific alteration assemblages and veinlet types are listed in Tables 4 and 5 and discussed below.

Chlorite-magnetite-albite alteration

The hydrothermal mineral assemblage chlorite-albite-magnetite (Table 4) is spatially associated with the intrusive centers and with the zone of >0.5 ppm Au. Mafic phenocrysts are completely replaced by fine-grained mixtures of chlorite and magnetite that destroy crystal forms. Plagioclase phenocrysts are partially replaced by albite, and the degree of albitization of plagioclase increases toward the outer edges of the orebodies. Calcite is abundant along the exposed south margins of the Verde West and Verde East (Fig. 6). Magmatic iron-titanium oxide minerals are oxidized to magnetite (± hematite)

TABLE 4. Types of Pervasive Hydrothermal Alteration at Refugio, Mineral Associations within Original Magmatic Mineral Sites

Alteration zone	Chl-mag-alb[1]	Py-alb-clay	Mag-ksp-olig[2]	Bio[2]
Alteration type	Chloritic	Intermediate argillic	Potassic	Potassic
Location and extent	Centered on ore, 100s meters	Mostly peripheral to ore district scale (3 km)	Centered on ore 100 m	Deep, lateral to ore 100s meters
Alteration minerals				
Hornblende sites	Chl-(mag)	Py-rt-kaol-ill	Mag-olig-qtz-bio *Chl*[3]	Bio-(mag) *Chl*[3]
Biotite sites	Chl-(mag)	Py-rt-kaol-ill	Mag-olig-qtz-bio *Chl*[3]	*Bio-(mag)* *Chl*[3]
Plagioclase sites	(Alb-cal)	Alb-(qtz-ksp)[4] Kaol-ill[3]	Olig *Ksp-qtz*[3]	*Olig-(bio-ksp)*
Ilmenite-magnetite grains	Mag-sph, Mag-rt[5] (Hm-rt)[3]	Py-rt	Mag-sph, Mag-rt[5] (Hm-rt[3]	Mag-sph, Mag-rt[5] (Hm-rt)[3]
Groundmass		Qtz-alb-kaol-ill	*Ksp-qtz-olig* *Chl*[3]	
Other minerals		(Cal) <1% tour[2]	(Spec)	
Opaque minerals	1–4% mag (Bn, cp, gl, mo)	0% mag	4–6% mag-cp-(hm[3]) 0.5–1% cp, (bn[6]) cp:py = >1:1	3-6% mag-cp-(hm[3]) <1% cp, (mo, sl) cp:py = <1:1
	<1% py[3]	2–4% py	<1% py[3]	<2% py[3]
Veins associated with alteration zones (in approx age sequence, see Table 5)	(1) Gar-chl-mag[1] (2) Banded qtz (3) Cal (4) (Qtz-alun)	(1) Banded qtz (2) Qtz-alun	(1) A-vnlts[2] (2) Banded qtz	(1) A-vnlts[2] (2) Banded qtz

Underline = major and/or complete replacement or most characteristic vein types; italics = partial replacement; parentheses = minor and/or trace occurrence

[1] Only at Verde
[2] only at Pancho
[3] relatively late
[4] relatively early
[5] replaces mag-sph
[6] not with py

Abbreviations: alb = albite,alun = alunite, apa = apaptite, bar = barite, bio = biotite, bn = bornite, cal = calcite, cas = cassitierite, chl = chlorite, cp = chalcopyrite, dias - diaspore, dick = dickite, ep = epidote, gar = garnet (andradite), gl = galena, gyp = gypsum, hm = hematite, ill = illite, kao = kaolinite, ksp = K-feldspar, mag = magnetite, mo = molybdenite, olig = oligoclase, qtz = quartz, rt = rutile, ser = sericite, sl = sphalerite, spec = specular hematite, sph = sphene, tour = tourmaline, vnlt = veinlet

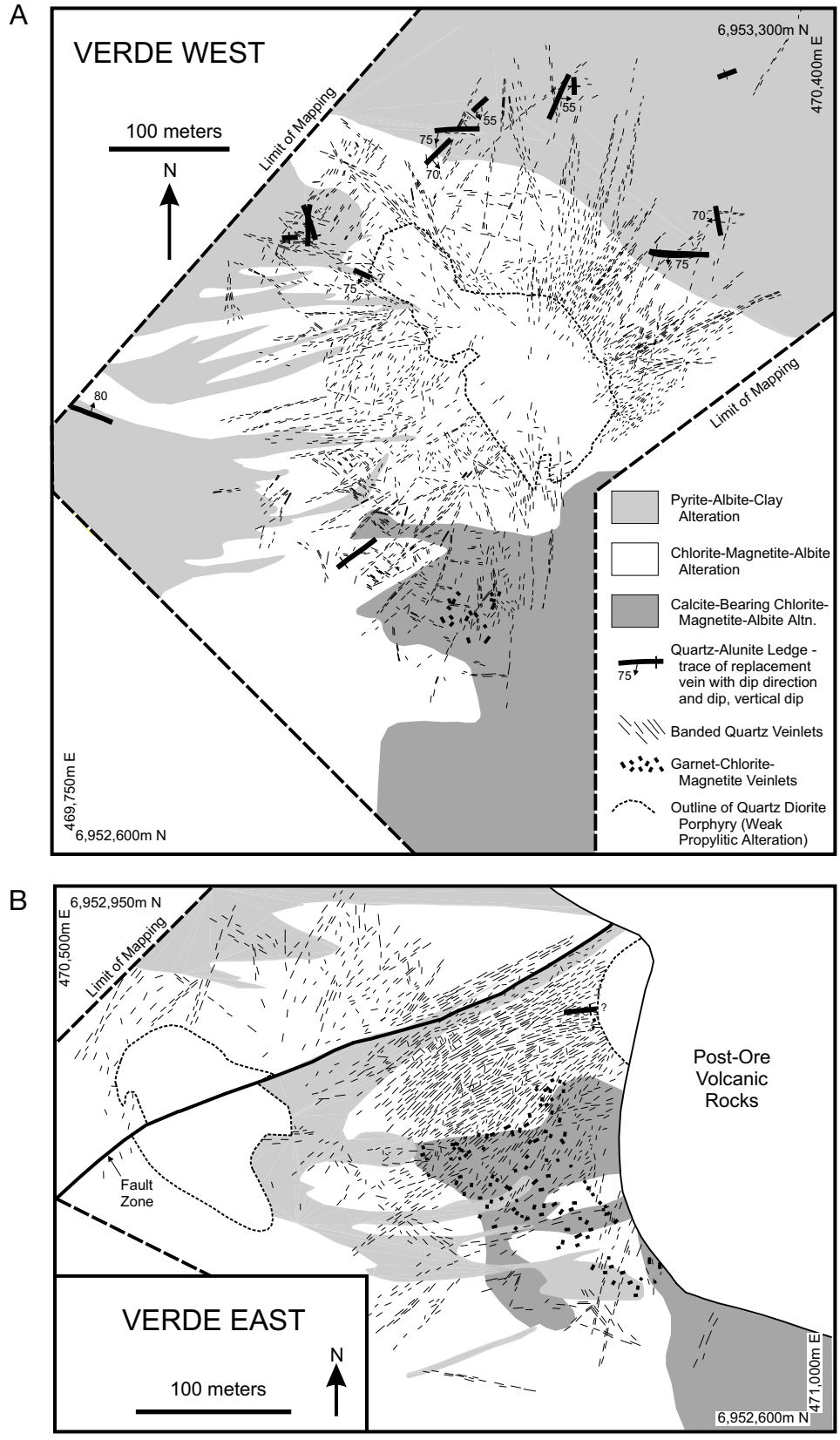

FIG. 6. Maps of hydrothermal alteration and vein types at the Verde orebodies, based on the present study. A. Verde West, not including unexposed southeastern portion. B. Southwestern exposed portion of Verde East.

+ rutile. Where in contact, chalcopyrite and magnetite have mutual boundaries and appear to have coprecipitated. Magnetite content is generally 1 to 4 vol percent, approximately equal to its abundance in weakly propylitized rocks throughout the district. Pyrite is present in minor amounts (<1 vol %) near the inner edges of the annular-shaped orebodies, and its abundance increases outward at the expense of magnetite. Where they are seen in contact in unweathered samples, pyrite rims or fills fractures in magnetite. Based on the above evidence, we assign pyrite to a younger and peripheral alteration event marked by pyrite-albite-clay (see below).

The characteristic texture of chloritized secondary biotite in potassically altered rocks of porphyry copper deposits, in which chlorite inherits the shreddy texture of hydrothermal biotite in hornblende phenocryst sites (Carten, 1987; Dilles and Einaudi, 1992), has only been detected in one core hole at Verde East where chlorite is associated with K feldspar. Our conclusion is that most of the Verde orebodies never underwent potassic alteration.

Andradite-chlorite-magnetite veinlets

Narrow, discontinuous veinlets with variable amounts of garnet, chlorite, and magnetite (Table 5), originally described by Rodriguez et al. (1997), are found in minor amounts throughout the zone of chlorite-magnetite-albite but are more common in the calcite-bearing zones along the margins of the orebodies (Fig. 6). The veinlets do not appear to have any spatial or temporal association with gold but locally contain sulfides, including pyrite, chalcopyrite, and traces of galena. The garnet is reddish brown and, based on electron microprobe analyses (Muntean, 1998), is a low aluminum, calcic garnet containing greater than 99 mole percent andradite. In most cases andradite is variably replaced by chlorite, magnetite, and unidentified clay, whereas magnetite is variably altered to hematite. The veinlets commonly have bleached white to gray alteration envelopes in which groundmass is variably replaced by quartz, mafic phenocrysts are altered to K feldspar, sphene, and albite-oligoclase, and chlorite is absent. The andradite veinlets cut volcaniclastic breccias and dacite porphyry. They cut and locally are cut by intrusive breccias, and they are absent in the late quartz diorite porphyry plugs. These relationships indicate that the veinlets formed episodically during the early stages of intrusive activity and during intense chlorite-albite-magnetite alteration.

Pyrite-albite-clay alteration

The outermost zone of pervasively bleached rocks consists of limonite (after pyrite), albite, illite, and kaolinite, and extends from Verde in a northwesterly direction over 3 km with a width of 2 km. It shows up as a strong color anomaly on aerial photographs and satellite images. Much of the kaolinite in bleached rocks is likely of supergene origin, as suggested by the presence of kaolinite veinlets associated with exotic limonite that cut across all other features. The pyrite-albite-clay zone (Fig. 6, Table 4) is defined by the absence of magnetite and chlorite and the presence of feldspars that were easily scratched and lacked cleavage. In unweathered drill core, the pyrite-albite-clay zone is pale greenish in color and contains about 2 to 4 vol percent pyrite. Plagioclase phenocrysts are mostly replaced by albite and by later clays, including kaolinite and illite. Illite, as referred to in this study, has a d(001) of 10 Å, and a crystal size less than about 5 μm. The groundmass and mafic mineral phenocrysts are replaced by quartz, albite, illite, kaolinite, pyrite, and rutile. Calcite is locally abundant in unweathered drill core, commonly occurring as narrow veinlets (<0.2 mm). The observed replacement textures suggest that pyrite-albite-clay alteration encroached inward onto the central chlorite-albite-magnetite zone.

Quartz-K feldspar-chlorite alteration of intrusive breccias

Alteration minerals in intrusive breccia generally are the same as the pervasive alteration assemblages described above, and no distinctive sulfide or iron oxide assemblages are present. However, locally, alteration led to interlocking grains of quartz and albite with clumps of K feldspar and chlorite, or irregular patches of granular quartz. In general, hydrothermal K feldspar and chlorite are more abundant in intrusive breccias than in other altered rock types at Verde.

Banded quartz veinlets

Banded quartz veinlets that occupy radial and concentric fractures described above are the hydrothermal feature most closely associated with gold ore at Verde (Fig. 7, Table 5). Veinlet abundances range up to 20 vol percent and are mostly between 1 to 4 percent at Verde West and 2 to 10 percent in the exposed parts of Verde East. The veinlets consist of quartz with a fine-grained (<0.25 mm) granular texture and local elongation perpendicular to the vein walls. Quartz fills hairline to millimeter-wide fractures (up to 2 cm wide) with slightly wavy walls that match up. Banded veinlets lack alteration envelopes, with relict plagioclase of magmatic composition commonly present directly against vein walls.

Many banded quartz veinlets contain dark gray bands that occur as symmetric pairs near the vein walls. The dark coloration is due to a high content of vapor-rich fluid inclusions and micrometer-sized magnetite grains (Fig. 7B). Dark bands locally show botryoidal textures that are continuous through quartz grains, suggesting that quartz recrystallized from a silica gel (e.g., Boydell, 1924; Ramdohr, 1980; Sander and Black, 1988). In addition to magnetite, dark bands contain rare micrometer-sized chalcopyrite, bornite, and sphalerite encapsulated in quartz.

Pyrite and minor calcite, K feldspar, sphene, magnetite, and chlorite commonly fill vuggy vein centers and constitute less than 5 percent of the veinlet volume. These minerals also fill fractures that cut the dark bands and locally extend out into wall rock. Late magnetite is coarser grained (up to 0.15 mm diam) than in the dark bands and is variably altered to hematite or pyrite.

Based on crosscutting relationships, most banded quartz veinlets formed during emplacement of the intrusive breccias and prior to intrusion of the quartz diorite porphyry stocks. The matrix of intrusive breccias encloses fragments of banded quartz veinlets and clasts of veined wall rock. However, the vast majority of the banded quartz veinlets cut both matrix and clasts, and the radial-concentric pattern of banded veinlets does not appear to be disrupted by bodies of intrusive breccia. The absence of veinlets in, and the truncation of veinlets by, quartz diorite porphyry indicates that banded

TABLE 5. Vein Types at Refugio (listed in order of decreasing relative age)

		Vein center or vein filling				
Vein type	Minerals	Major	Minor	Thickness	Length	Structure
Garnet[1]	Gangue	Gar-chl	Qtz, cal, alb-olig, ep, sph, apa	<0.5 mm	10s cm	Discontinuous, irreg walls
	Opaque	Mag	Py, cp, gl			
A-veinlets						
A-1[2]	Gangue	Bio-qtz		<0.2 mm	cms	Discontinuous, irreg walls
	Opaque	Mag-cp	Py, sl			
A-2[2]	Gangue	Qtz	Chl, apa	<0.2 mm	cms	Discontinuous, irreg walls
	Opaque	Mag-cp				
A-3[2]	Gangue	Qtz	Chl, bio, bar	<1–2 mm	10s cm	Continuous straight walls
	Opaque	Mag-cp	Bn, spec			
A-4[2]	Gangue	Qtz		<1–2 mm	10s cm	Continuous straight walls
	Opaque	Cp	Py			
Banded qtz	Outside dark bands:					
	Gangue	Qtz-ksp-cal-chl	Ill, ep, gar, gyp	mms–	10s cm	Continuous, wavy walls
	Opaque	Py, Mag	Cp, sl, gl, mo, cas	2 cm	to m's	
	In dark bands:					
	Gangue	Qtz		0.001–	10s cm	Symmetric pairs
	Opaque	Mag	Cp, bn, sl	0.1 mm	to m's	
D veins[2]						
	Gangue	Qtz		<1 mm–	1-10 m	Continuous
	Opaque	Py	Cp, mo	3 cm		
Qtz-alunite						
	Gangue	Qtz-alun	Rut, dick, dia, bar	0.5–	10s–	Continuous, replacement, bx common
	Opaque	Py		40 m	150 m	

		Wall-rock alteration halo			Age relative to other veins		Age relative to intrusions	
Vein type	Minerals	Major	Minor	Thickness	Postdate	Predate	Postdate	Predate
Garnet[1]	Gangue	Qtz	Ksp-sph-alb	0.5–5 mm		Banded vnlts	Dacite por intrus bx	
	Opaque		Mag, py					Intrus bx qtz-dior por[1]
A-veinlets								
A-1[2]	Gangue	Bio, or		<0.1 mm	A-3	A-2, 3, 4, banded	Intrus bx	(Intrus bx)
	Opaque	Ksp-olig				vnlts, D vns	qtz-dior por	
A-2[2]	Gangue	Ksp-Qtz		<0.1 mm	A-2, 3	A-3, 4, banded	Intrus bx	(Intrus bx)
	Opaque					vnlts, D vns	qtz-dior por	
A-3[2]	Gangue	None	None		A-4, (A-1, 2)	A-4, banded	Intrus bx	(Intrus bx)
	Opaque					vnlts, D vns	qtz-dior por	
A-4[2]	Gangue	None	None			Banded vnlts,	Intrus bx	(Intrus bx)
	Opaque					D vns	qtz-dior por	
Banded qtz	Outside dark bands							
	Gangue	None	None		Garnet vnlts		Dacite por	
	Opaque				A-vnlts		intrus bx	(Intrus bx)
	In dark bands:						qtz-dior por	qtz-dior por[1]
	Gangue	None	None			D vns		
	Opaque					Qtz-alunite[1]		
D veins[2]								
	Gangue	Qtz-ser		1–5 cm	A-vnlts,	Qtz-alunite ?	Dacite por	
	Opaque	Py			banded vnlts		intrus bx	
							qtz-dior por	
Qtz-alunite								
	Gangue	Qtz-kao	Ser	m	Banded vnlts[1]		Dacite por	
	Opaque	Py					intrus bx	

[1] Relationship seen at Verde only
[2] Relationship seen at Pancho only
Abbreviations as in Table 4; additional abbreviations: bx = breccia, dior = diorite, dk = dark, intrus = intrusive, irreg = irregular, porph = porphyry; relative age of qtz-alunite veins and quartz diorite porphyry is uncertain; relative age of D veins and qtz-alunite veins is uncertain

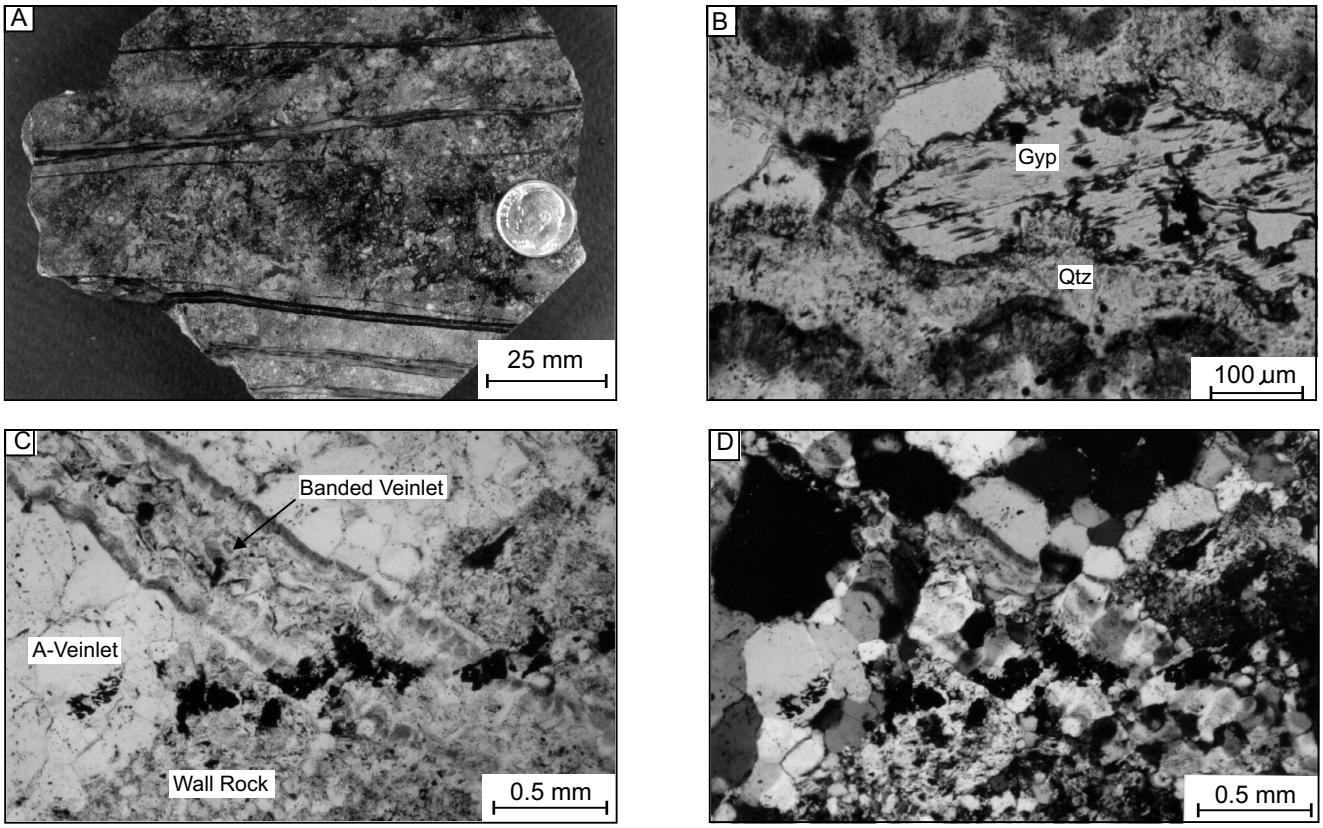

FIG. 7. Banded quartz veinlets. A. Subparallel banded quartz veinlets hosted by intrusive breccia from Verde West. B. Photomicrograph of banded veinlet from Verde West showing botryoidal banding, uncrossed polars. Dark bands contain abundant micron-sized magnetite and vapor-rich fluid inclusions. The mineral with the cleavages in the vuggy vein center is gypsum with pyrite inclusions. C. Quartz-magnetite-chalcopyrite A-veinlet from Pancho cut by banded quartz veinlet, uncrossed polars. Note botryoidal nature of the bands. D. Same as C, crossed polars. Note how banded vein material occurs as overgrowths on the earlier granular quartz of the A-veinlet, the continuity of bands through quartz crystals, and how the fine-grained quartz of the interior of the banded veinlet contrasts with the coarser granular quartz of the A-veinlet.

quartz veinlets had essentially ceased to form by the time the stocks were emplaced at their present structural level. Banded quartz veinlets cut and offset garnet-chlorite-magnetite veinlets; the reverse crosscutting relationship has not been observed in spite of the fact that both vein types appear to have formed through most of the intrusive activity prior to emplacement of quartz diorite porphyry.

Quartz-alunite ledges

Replacement veins of quartz-alunite alteration are most abundant between the Pancho and Verde orebodies where they are up to 150 m long and 40 m wide. The vast majority of the quartz-alunite ledges in the district are present above the 4,300-m elevation. Quartz-alunite ledges commonly are anomalous in gold, but gold grades greater than 1 ppm have not been reported.

At Verde, quartz-alunite ledges are mostly found on the periphery and outer edges of the Verde West orebody (Figs. 6 and 8, Table 5), where they have widths of less than a meter, lengths of tens of meters, and dips greater than 55°. Host rocks are completely altered to quartz + alunite + pyrite + rutile ± dickite ± diaspore, original rock textures are mostly destroyed, but vuggy residual quartz is rare. The amount of quartz decreases outward from the center of the ledges, and a zone of quartz-kaolinite-sericite alteration forms an outer halo in which original rock textures are mostly preserved.

Within the central quartz-alunite zone, alunite occurs as aggregates of fine-grained (10–50 μm) crystals and as blades as long as 200 μm in length. X-ray diffraction patterns indicate a significant natroalunite component. Original pyrite content, based on an estimation of leached cavities and rare unoxidized zones, was approximately 5 vol percent. In unoxidized zones pyrite is intergrown with alunite with smooth grain boundaries. Late fractures are filled with alunite + pyrite, diaspore + pyrite, or barite.

Where quartz-alunite ledges intersect zones of banded quartz veinlets, diaspore and alunite veinlets cut banded quartz veinlets (Fig. 9C, D). In addition, gangue minerals besides quartz and pyrite in banded quartz veinlets are absent, the boundaries of quartz veinlets are less distinct, and dark bands are subdued. These observations indicate that the quartz-alunite ledges postdate the banded quartz veinlets. The relative age of quartz-alunite ledges and the late quartz diorite porphyry stocks at Verde remains undocumented because of the lack of critical exposures at the time of this study.

Textural evidence for equilibrium between pyrite and alunite, the coarse, bladed nature of the alunite, and the association of alunite with dickite and diaspore are consistent with

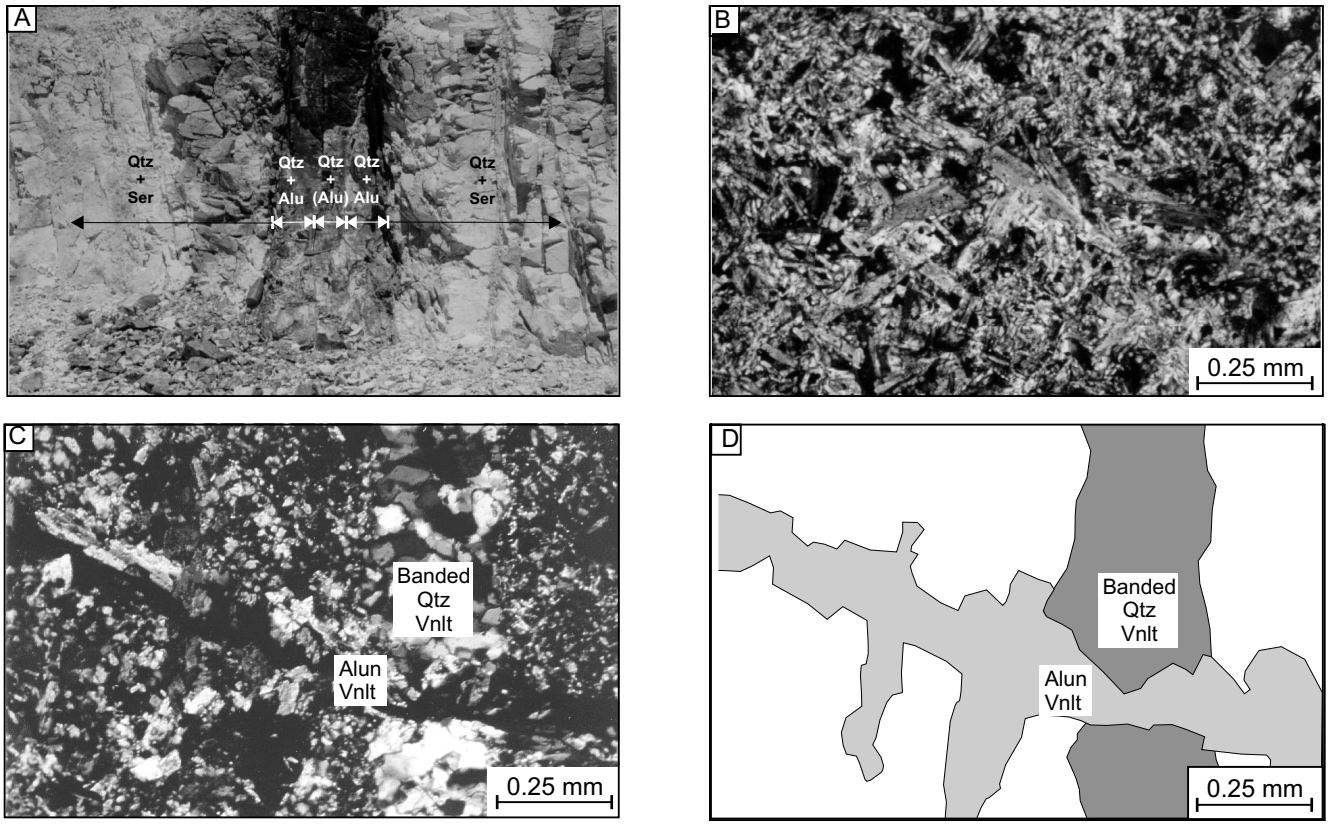

FIG. 8. A. Exposure of quartz-alunite ledge in road cut from Verde West. The ledge zones outward from a central, 25-cm-thick quartz-rich zone to quartz + alunite to quartz + sericite alteration. B. Photomicrograph of quartz-alunite ledge from Pancho, showing coarse, bladed alunite intergrown with quartz. C, D. Alunite veinlet in ledge cutting banded quartz veinlet.

a hypogene origin for the alunite (cf. Hemley et al., 1969). Stable isotope studies of similar alunite occurrences elsewhere have shown that such alunite forms from magmatic vapor condensed into meteoric water at temperatures typically greater than 200°C; such alunite is termed magmatic-hydrothermal alunite (Rye et al., 1992; Arribas, 1995). The presence of dickite, rather than pyrophyllite, suggests temperatures less than 260°C (Hemley et al., 1980).

Gold occurrence

Gold grades of surface samples correlate closely with the mapped abundance of banded quartz veinlets (Figs. 6 and 8). Gold grades at Verde West form a structurally controlled, starburstlike pattern that reflects the radial and concentric distribution patterns of veinlets. A similar pattern is present in the exposed part of Verde East, although zones containing >1 ppm gold at Verde East are larger and more continuous because of the higher abundance of banded veinlets. Gold is centered in the late stocks of quartz diorite porphyry, which sharply truncate ore zones (>0.5 ppm gold) at Verde East and Verde West. At Verde West ore zones locally extend into quartz diorite porphyry along fault zones or in sheeted sets of banded quartz veinlets along the margins of the stock. Pyrite-albite-clay alteration forms a narrow (10–50 m) halo to the Verde East orebody, whereas it forms an incomplete, broader halo on the western, northern, and eastern margins of the Verde West orebody, overlapping considerably with ore zones along the northeastern and eastern margins. Zones with >0.05 ppm gold extend about 100 m beyond the outer limits of banded veinlets at both Verde West and Verde East.

Eleven observations of gold in four samples support the correlation between gold grades and banded quartz veinlets (Fig. 10). Gold occurs within veinlets or in wall rock along the margins of veinlets. A few grains of gold were found with magnetite in the dark bands, where gold and magnetite occur as free, distinctly round, <10-μm grains encapsulated in quartz (Fig. 10A, B). Most of the gold grains observed in the banded quartz veinlets are closely associated with pyrite that fills fractures that postdate the dark bands. In these occurrences, gold occurs mostly as free grains along quartz grain boundaries and in contact with pyrite and chlorite (Fig. 10C, D). Three gold grains were found in illite, chlorite, and K feldspar in wall rock within micrometers of the margins of banded veinlets (Fig. 10E, F). Gold found with the pyrite or gangue minerals in the veinlets or along the margins of the veinlets is interpreted to have formed after the dark bands and during the late stages of filling in of banded quartz veinlets. Based on electron microprobe analyses, the average gold/silver ratio of gold associated with the magnetite in the dark bands is 99:1 (by wt, 2 analyses), whereas the average gold/silver ratio of gold associated with pyrite or gangue minerals is 91:9 (4 analyses; Muntean, 1998).

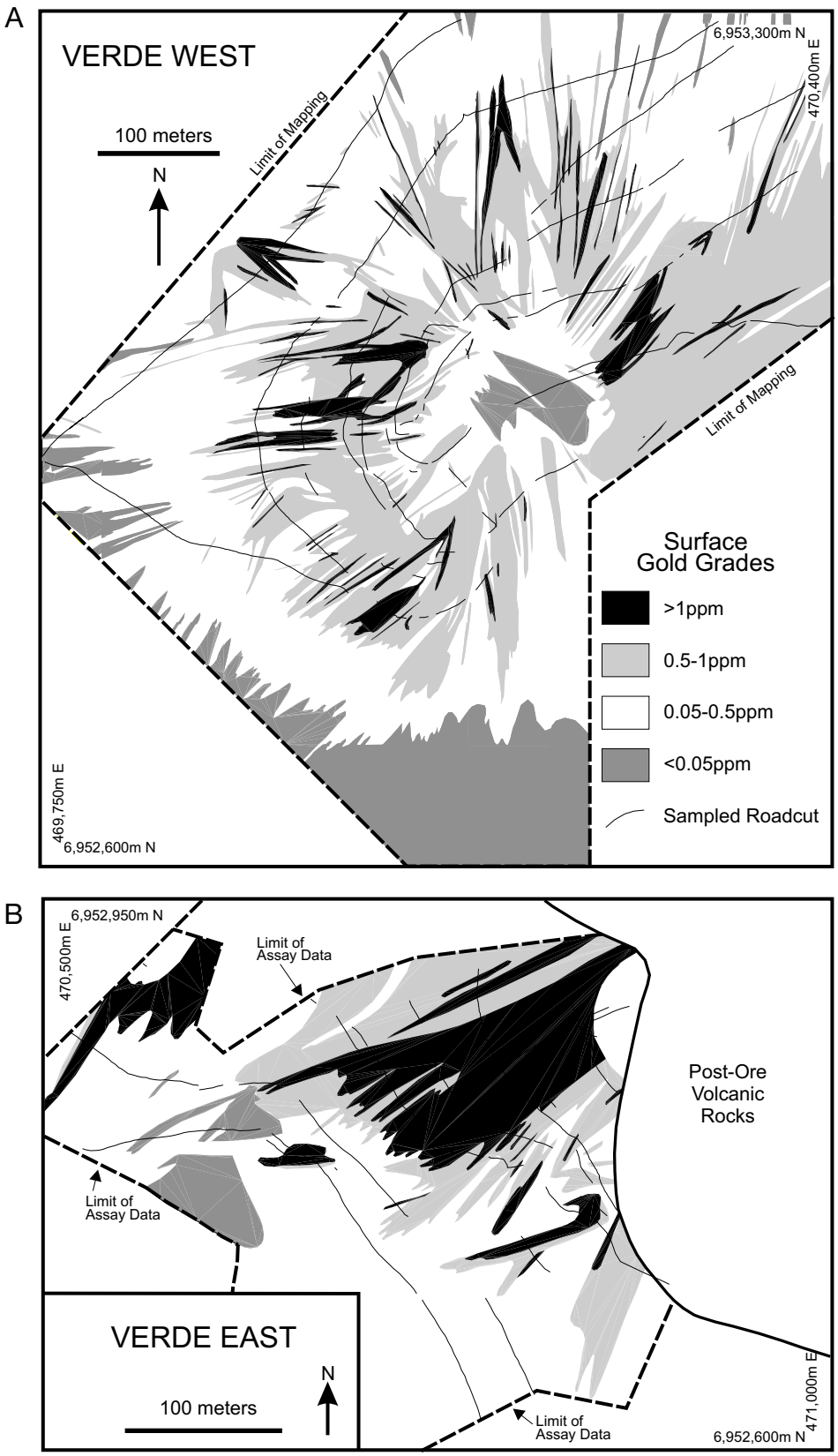

FIG. 9. Maps showing distribution of surface gold grades at the Verde orebodies, based on 2-m channel samples of the drill roads. A. Verde West, not including unexposed southeastern portion. B. Southwestern exposed portion of Verde East.

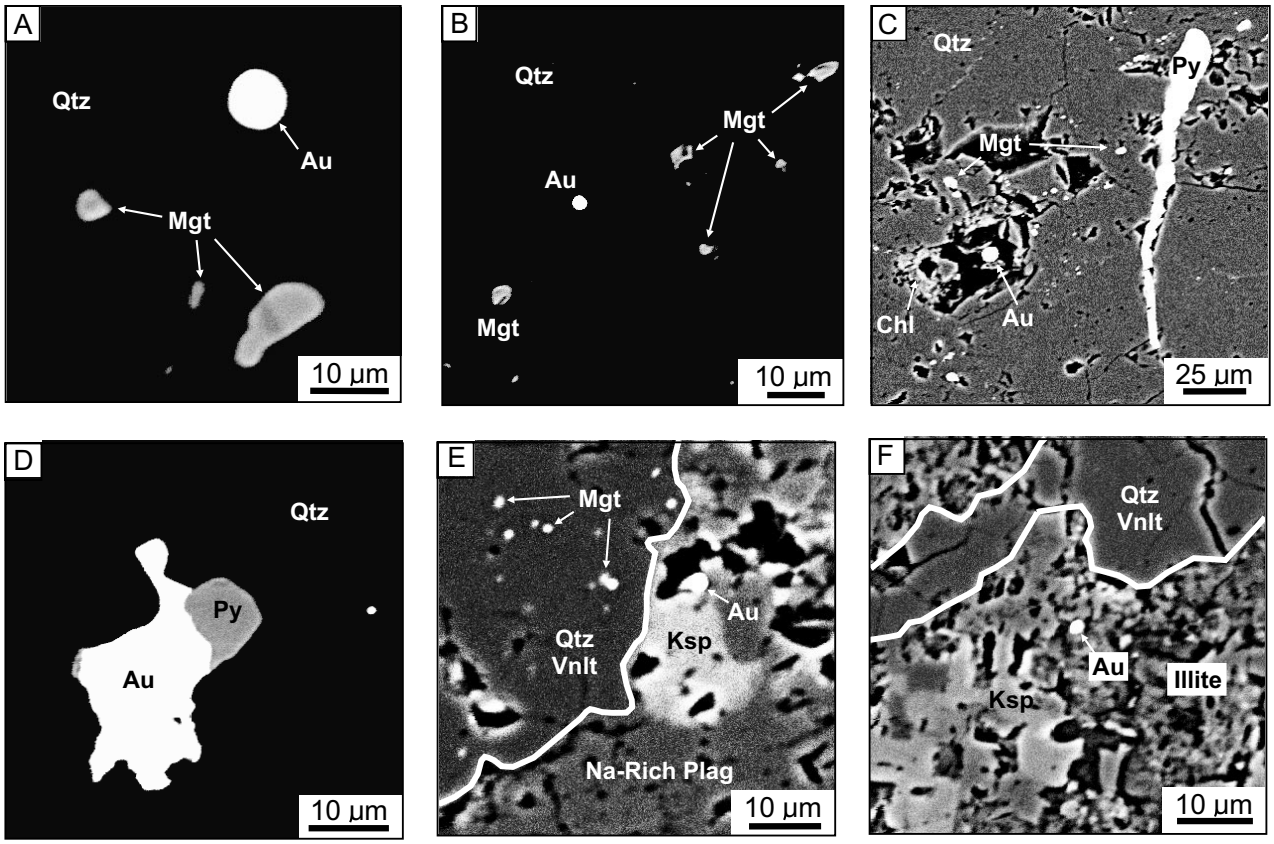

FIG. 10. Back-scattered electron images of gold occurrences in banded quartz veinlets at Verde. Abbreviations: Au = native gold, Chl = chlorite, Ksp = K feldspar, Mgt = magnetite, Na-Rich Plag = Na-rich plagioclase, Py = pyrite, Qtz = quartz. A, B. Gold with magnetite from dark band in banded quartz veinlet. Note round morphology of the grains. C. Gold grain in patch of chlorite outside dark bands in banded quartz veinlet. D. Relatively coarse gold attached to pyrite outside dark bands in banded quartz veinlet. E. Gold with K feldspar along margin of a banded quartz veinlet. F. Gold in patch of illite inside outer margin of quartz veinlet.

Pancho Gold Deposit

In addition to containing hydrothermal features similar to those at Verde, Pancho also contains alteration and veinlet styles that are similar to those observed in porphyry copper deposits. Thus, Pancho may serve as a link between porphyry copper and porphyry gold deposits. Geologic mapping of exposures along a 30° to 40° slope over a vertical interval of about 400 m yields a plan map that can also be viewed as a distorted cross section with up to the east (Figs. 11 and 12).

Intrusions and structure

The highest gold grades at Pancho are centered on a quartz diorite porphyry stock with a diameter of at least 900 m (Figs. 3 and 11) and an east-trending zone of abundant quartz veinlets 1.1 km long and 0.7 km wide (Figs. 3 and 12). The quartz diorite porphyry stock is cut by steeply dipping dikes of intrusive breccia that strike N 50° to 70° W. Most faults at Pancho are parallel to the dikes and are interpreted to have small, normal displacements. A secondary set of N 70° to 80° E-striking faults appears to be associated with larger east-northeast-trending faults that bound the northeastern and southern sides of Pancho (Fig. 3). The two fault sets appear to crosscut each other. Banded quartz veinlets locally form steeply dipping, northwest-trending sheeted sets that are parallel to dikes and faults, and, unlike Verde, the veinlets do not exhibit a radial and concentric pattern.

Magnetite-K feldspar-oligoclase zone

The potassic alteration assemblage of magnetite-K feldspar-oligoclase forms a zone about 200 m in diameter in the center of the deposit (Fig. 12, Table 4). Here, only minor relics of primary magmatic minerals survived the alteration process. Plagioclase phenocrysts are mostly altered to oligoclase. Mafic mineral phenocrysts are completely altered to magnetite, oligoclase, quartz, and minor shreddy biotite that in some samples is partly replaced by chlorite. K feldspar, quartz, oligoclase, and minor chlorite, the latter possibly an overprint on secondary biotite, replace primary groundmass. Local patches of K feldspar and quartz replace both groundmass oligoclase and the rims of oligoclase-altered phenocrysts, resulting in partial destruction of primary rock texture. Opaque minerals include 3 to 5 vol percent disseminated magnetite that is partly oxidized to hematite and <1 vol percent chalcopyrite. Specular hematite is locally present, and magmatic ilmenite is replaced by magnetite, sphene and/or rutile.

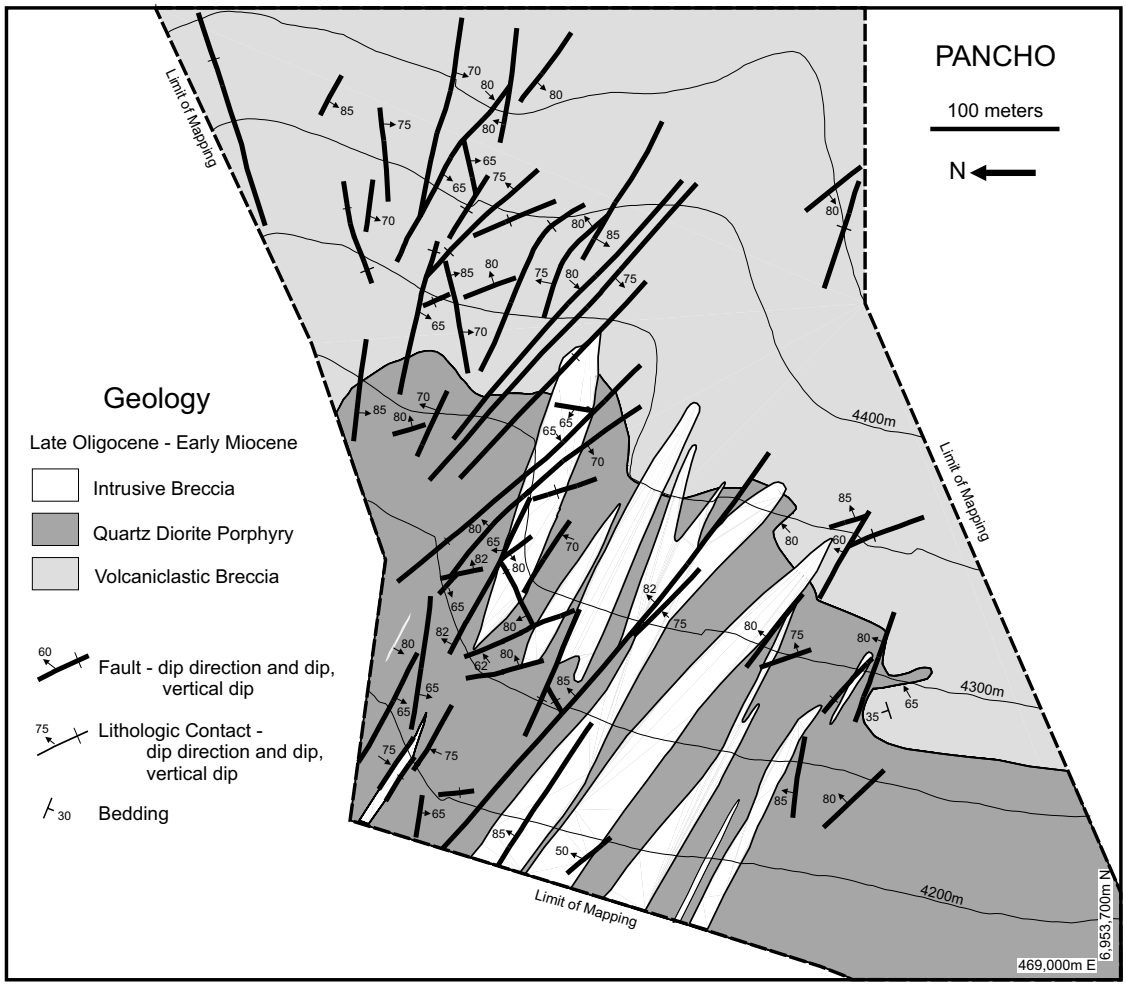

FIG. 11. Geologic map of the Pancho orebody, based on the present study. Given the steep topography, the map is arranged so that north is to the left allowing the map to be viewed as a distorted cross section.

Biotite zone

The magnetite-K feldspar-oligoclase zone changes gradually laterally and downward to a zone of abundant brown secondary biotite with only traces of secondary K feldspar (Fig. 12, Table 4). In deep exposures, the biotite zone grades laterally to district-scale weak propylitic assemblages. Shreddy aggregates of biotite completely replace magmatic hornblende and partially replace magmatic biotite. Based on electron microprobe analyses, the Fe/(Fe + Mg) mole ratio of secondary biotite and relict magmatic biotite ranges from 0.17 to 0.26 (Muntean, 1998). Plagioclase phenocrysts are variably altered to oligoclase and locally minor biotite and K feldspar. Two to 5 vol percent magnetite and <2 vol percent chalcopyrite occur with secondary biotite as disseminations and in altered mafic mineral sites; pyrite occurs in late fractures. There is an inverse relationship between the pyrite and magnetite + chalcopyrite contents.

In areas that underwent potassic alteration, secondary biotite and relict biotite phenocrysts are variably altered to chlorite. Locally, this late chloritic alteration, consisting of chlorite-albite (oligoclase)-quartz-leucoxene, was intense and destroyed rock textures.

A-veinlets

Sets of early quartz-magnetite-sulfide veinlets, here termed A-veinlets (cf. Gustafson and Hunt, 1975), are associated spatially with potassically altered rocks and are restricted to intrusive rocks (Figs. 12 and 13, Table 5). A-veinlets, mostly constituting less than 2 vol percent of the rock, range in character from generally older, discontinuous, and irregular hairline streaks with variable amounts of magnetite, biotite, quartz, and minor chalcopyrite, to generally younger, more continuous, wider veinlets with magnetite and/or chalcopyrite. The younger, more continuous veinlets contain more quartz and chalcopyrite than older, discontinuous veinlets. The older, discontinuous A-veinlets commonly have alteration envelopes of K feldspar or biotite, whereas younger A-veinlets lack megascopic alteration halos. Quartz is pale gray and has a distinct sugary texture in hand sample. Pyrite occurs in some A-veinlets on the outer margins of the deposit. Where pyrite and magnetite are present together, textures indicate replacement of magnetite by pyrite. The progression from discontinuous hairline streaks to more continuous, wider veinlets suggests more sustained brittle behavior with time. However, discontinuous varieties locally crosscut the

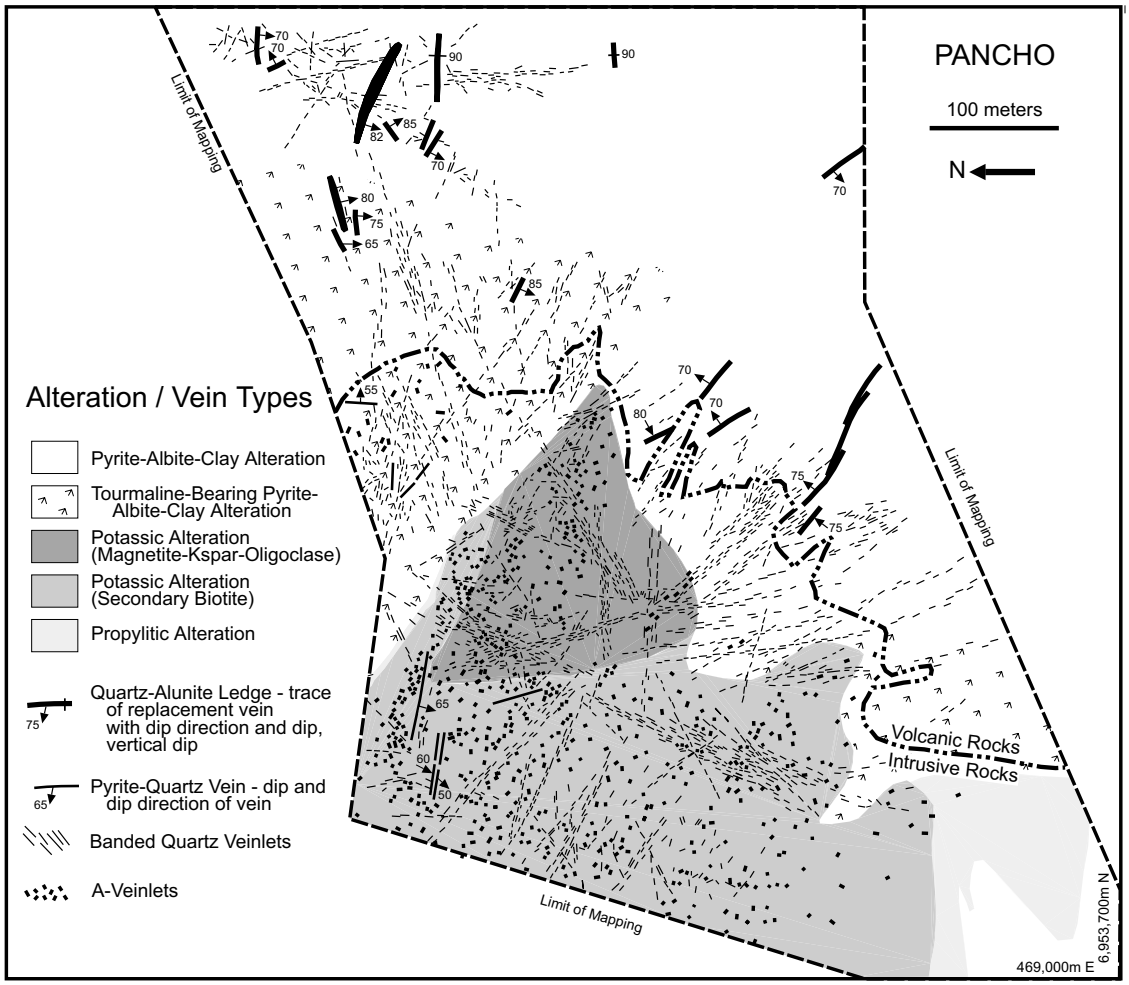

FIG. 12. Map of hydrothermal alteration and vein types at Pancho, based on the present study.

more continuous, wider veinlets, suggesting A-veinlets could have formed in a cyclical fashion as noted at El Salvador (Gustafson and Hunt, 1975).

Banded quartz veinlets

Banded quartz veinlets (Fig. 12, Table 5) that are similar to those at Verde are more abundant than A-veinlets at Pancho. Banded veinlets constitute around 2 to 5 vol percent of the rock, culminate at 10 vol percent in the upper levels of the quartz diorite porphyry stock, and are widespread in the overlying volcanic rocks where A-veinlets are absent. Banded veinlets cut and offset A-veinlets (Fig. 13B). Although the reverse relationship has not been found, the distinction between banded veinlets and the wider, more continuous, quartz-rich A-veinlets is locally difficult to make. Episodic perturbations may have occurred during the formation of A-veinlets that resulted in abrupt transitions to conditions conducive for the formation of the dark bands. As at Verde, formation of banded quartz veinlets overlapped in time with emplacement of intrusive breccia dikes.

Pyrite-albite-clay alteration

Potassic alteration is increasingly overprinted at high elevations by pervasive pyrite-albite-clay alteration, similar to that seen at Verde. The upper limit of the potassic alteration zones shown in Figure 12, within 100 m of the overlying volcanic rocks, was defined indirectly by the presence of shreddy textures in mafic phenocryst sites and/or the presence of A-veinlets. The intensity of pyrite-albite-clay alteration increases with elevation and distance from the quartz diorite intrusion. Plagioclase phenocrysts, mostly replaced by albite, were subsequently replaced by kaolinite and local minor quartz and illite. The groundmass and mafic mineral phenocrysts are completely replaced by variable amounts of kaolinite, pyrite, rutile, illite, albite, and quartz. Pyrite abundance, based on unoxidized samples and leached cavities, is mostly 2 to 4 vol percent. Locally, specular hematite is present instead of pyrite. Up to about 1 vol percent dark green tourmaline is present as disseminated rosettes in the lower parts of the pyrite-albite-clay zone near its contact with potassic alteration. Where there are banded quartz veinlets, kaolinite with local pyrite fills fractures that cut across the veins, suggesting

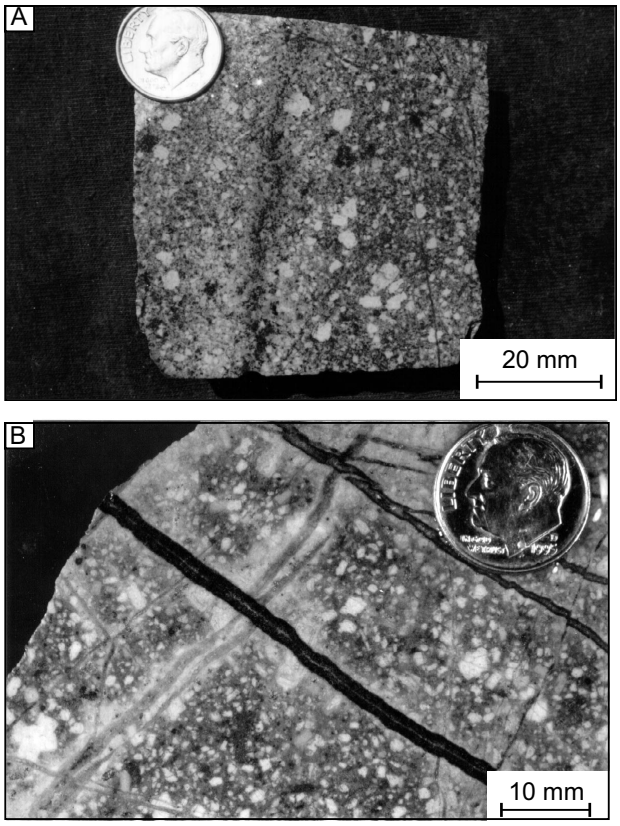

FIG. 13. Core samples showing A-veinlets from Pancho orebody. A. Magnetite-quartz-chalcopyrite veinlet with diffuse K feldspar-quartz alteration envelope within pervasive magnetite-K feldpsar-oligoclase alteration zone in quartz diorite porphyry. B. Greater than one generation of banded quartz veinlets cutting and offsetting A-veinlets within pervasive magnetite-K feldspar-oligoclase alteration zone in quartz diorite porphyry. Apparent alteration envelopes are the result of supergene alteration.

that the pyrite-albite-clay alteration is younger. Nevertheless, broadly contemporaneous but spatially separate formation of banded quartz veinlets and pervasive pyrite-albite-clay alteration cannot be ruled out.

Pyrite-quartz-sericite veins

Pyrite-quartz veinlets with quartz-sericite-pyrite alteration envelopes (pyrite-quartz-sericite veins), similar to the D veins described by Gustafson and Hunt (1975) at El Salvador, are present locally in the potassic zones and in the lower parts of the pyrite-albite-clay zone (Fig. 12, Table 5). Vein fillings range up to several centimeters in width but commonly form anastomosing networks of narrow, vuggy veinlets with slightly wavy walls. They contain between 10 and 60 vol percent pyrite with local (<1 vol %) chalcopyrite and/or molybdenite. Quartz has a granular texture and commonly is elongated perpendicular to the vein walls. Comb-textured quartz is locally present. Alteration envelopes are up to several centimeters wide and the intensity of alteration decreases gradually away from the vein. Where crosscutting relationships were observed, pyrite-quartz-sericite veins cut and offset A-veinlets and banded quartz veinlets. Pyrite-quartz-sericite veins clearly postdate potassic alteration, but their temporal relationship to pyrite-albite-clay alteration is unclear. We have not seen pyrite-quartz-sericite veins truncated at intrusive contacts and, therefore, conclude that these veins formed after all intrusions had been emplaced.

Quartz-alunite ledges

Quartz-alunite ledges, consisting of mixtures of quartz, alunite, and minor rutile (Table 4), are restricted to zones of pervasive pyrite-albite-clay alteration in the volcanic rocks at high elevations (Figs. 9 and 12, Table 5). Leached cavities indicate an original pyrite content of about 4 to 7 vol percent, and relict pyrite occurs locally as inclusions in quartz and alunite. As at Verde, the ledges contain anomalous gold grades but do not constitute ore. The ledges at Pancho are brecciated locally, containing matrix-supported, subangular rock fragments in a locally vuggy rock-flour matrix.

Gold occurrence

Gold was not directly observed at Pancho. However, its paragenesis can be deduced from the pattern of surface gold grades (Fig. 14). A fairly continuous zone of gold grades between 0.5 and 1 ppm coincides closely with pervasive potassic alteration and A-veinlets in the intrusive rocks. Gold grades of >1 ppm occur where there are sets of sheeted banded quartz veinlets. The highest grades in the intrusive rocks also coincide with pervasive magnetite-K feldspar-oligoclase alteration. Zones with gold contents greater than 0.5 ppm in the overlying volcanic rocks are mostly less than 10 m wide and are associated directly with sets of sheeted, banded quartz veinlets that decrease in abundance with increasing distance from the intrusion. Zones of >0.05 ppm gold extend to about 150 m beyond the outer limits of banded quartz veinlets.

Fluid Inclusions in Banded Quartz and A-veinlets

A reconnaissance fluid inclusion study was undertaken to compare the petrographic characteristics, origin, and general range of homogenization temperature and salinity of fluid inclusions in banded quartz veinlets and A-veinlets. An additional objective was to estimate the depths of formation of Verde and Pancho. Fluid inclusion types recognized, following the classification scheme of Nash (1976), are type I (liquid-dominant inclusions without halite daughters), II (vapor-dominant inclusions without halite daughters), and IIIa (liquid-dominant inclusions with halite daughters that homogenize by bubble disappearance). Type II inclusions were abundant in all samples of banded quartz veinlets and A-veinlets; we interpret their abundance and ubiquity as evidence for widespread, continuous boiling at both deposits. Data were collected from fluid inclusion assemblages (cf. Goldstein and Reynolds, 1994) that contained liquid- (types I or IIIa) and vapor-dominant inclusions (type II). Fluid inclusion assemblages are groups of cogenetic fluid inclusions that were trapped in a growth zone in quartz (primary fluid inclusions) or along a healed fracture (secondary fluid inclusions). Microthermometric data were collected only from types I and IIIa inclusions, using a U.S. Geological Survey gas-flow heating/freezing stage adapted by Fluid Inc. Explanation of methodology, sample descriptions and locations, and individual fluid inclusion measurements, including interpretation of groups of measurements in terms of fluid inclusion assemblages, are found in Muntean (1998).

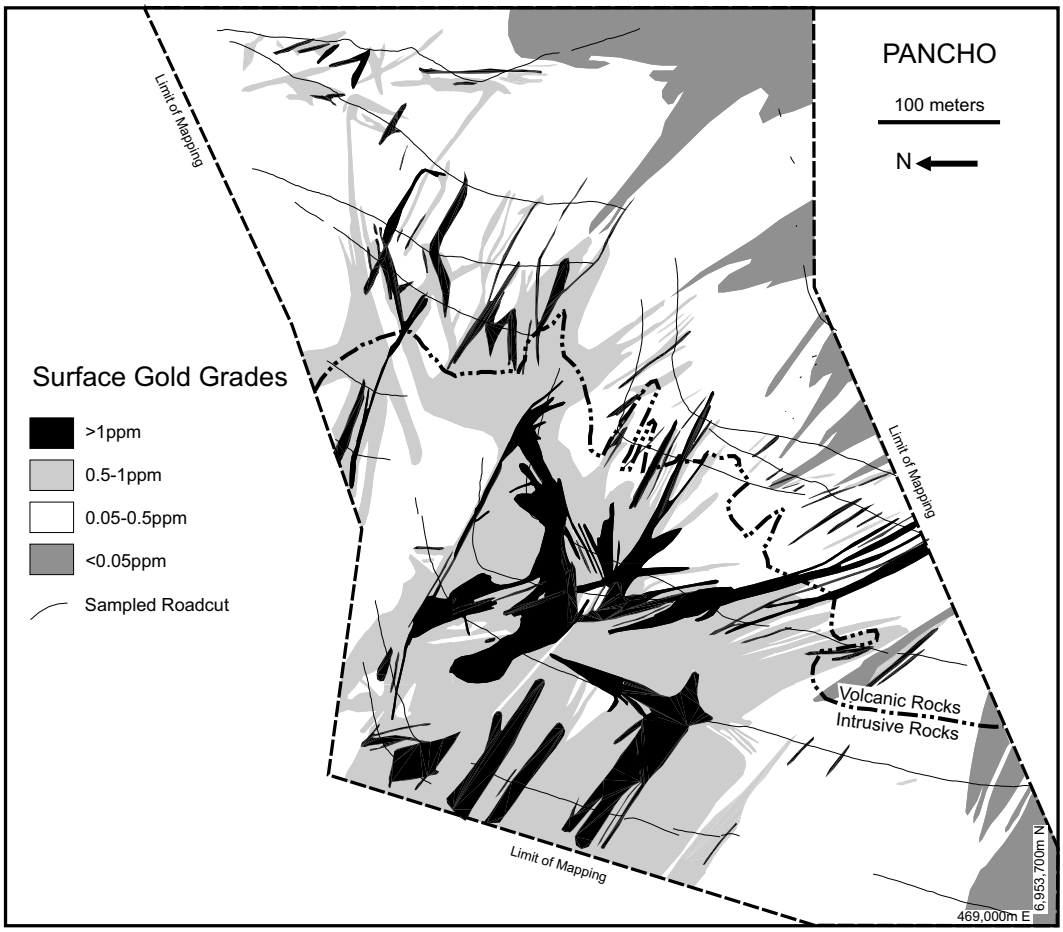

FIG. 14. Map showing distribution of surface gold grades at Pancho, based on 2-m channel samples of the drill roads.

Fluid inclusions in banded quartz veinlets

Over 99 percent of the fluid inclusions in banded veinlets from Verde and Pancho are type II inclusions with no recognizable liquid (Fig. 15). Less than 1 percent of the fluid inclusions are liquid rich, either type IIIa or, less commonly, type I inclusions with small (10–25 vol %) vapor bubbles. The proportion of vapor- to liquid-rich inclusions is the same inside and outside the dark bands, but the dark bands have more abundant inclusions and many are submicron in size. Both liquid- and vapor-rich fluid inclusions have mostly rounded negative crystal shapes. Vapor-rich inclusions range up to a 50-μm diam, whereas liquid-rich inclusions range up to a 25-μm diam. In addition to ubiquitous halite, a few type IIIa inclusions contain sylvite(?), insoluble opaque crystals, and insoluble, hexagonal to prismatic crystals that are pale green, birefringent, and high relief (possibly an iron chloride mineral; cf. Cox, 1985). Coexisting vapor- and liquid-rich inclusions occur in growth zones represented by the dark bands (Fig. 15A, B) and on either side of the dark bands (Fig. 15C), where they are interpreted as primary with respect to crystallization of gel to quartz. Coexisting vapor- and liquid-rich inclusions also occur in secondary planes that cut growth zones (Fig. 15D).

Homogenization temperatures from eight fluid inclusion assemblages of types I or IIIa inclusions coexisting with type II inclusions in three samples from Verde are 220° to 350°C and salinities are 3.4 to 34 wt percent NaCl equiv (Fig. 16). Homogenization temperatures represent actual trapping temperatures because these inclusions were trapped with type II inclusions along the liquid + vapor curve. No systematic difference was observed between the homogenization temperatures and salinities from growth zones represented by the dark bands and growth zones on either side of the dark bands. Fluid inclusions with salinities less than 17.5 wt percent NaCl equiv occur in secondary planes but yield the highest homogenization temperatures. In a few fluid inclusion assemblages, type I inclusions could not be frozen, suggesting that the inclusion fluids may be near halite saturation and unable to nucleate ice because of kinetic effects (T.J. Reynolds, pers. commun., 1997). First melting of ice was recognized as low as –56°C, indicating the presence of divalent ions such as Ca^{2+}, Mg^{2+}, and/or Fe^{2+} (Goldstein and Reynolds, 1994). Type II inclusions do not contain any recognizable liquid CO_2. No evidence for CO_2 was found during cooling to –125°C and subsequent heating to –56.6°C (the melting point of liquid CO_2).

Fluid inclusions in A-veinlets

Type IIIa inclusions with ubiquitous multiple daughter minerals are limited to A-veinlets at Pancho and coexist with

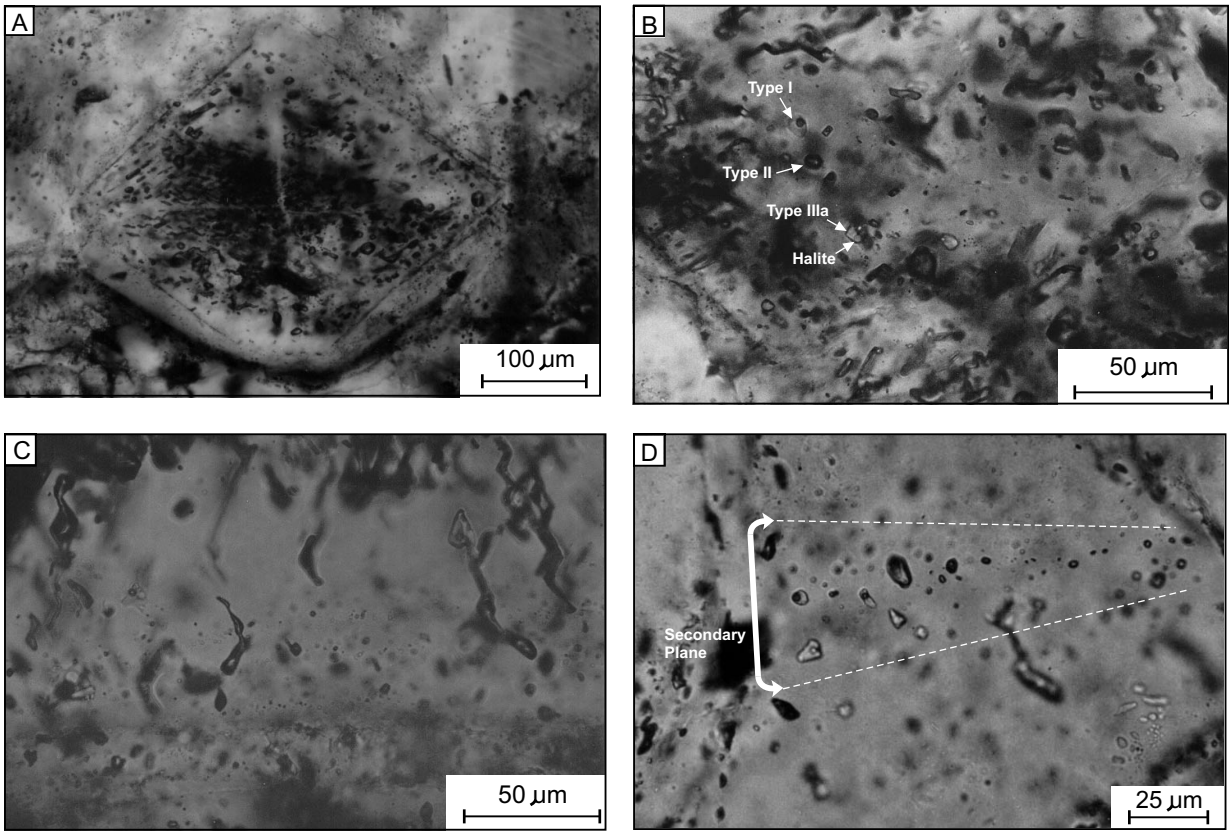

FIG. 15. Photomicrographs of fluid inclusions in banded quartz veinlets. A. Quartz crystal (c-axis is at a high angle to the field of view) from Verde West within a dark band cored by primary type II vapor-rich inclusions. B. Dark band showing abundant large dark type II vapor-rich inclusions and minor type I and IIIa liquid-rich inclusions. The dark areas are probably due to submicron-sized fluid inclusions. Sample is from Verde West (RV027). C. Growth zone between vein wall (just below the field of view) and dark band (dark areas near top of view), showing dark, vapor-rich type II inclusions coexisting with minor type IIIa liquid-rich inclusions. The vapor-rich inclusions were trapped along the crystallographic planes of the quartz. Sample is from Verde West (RV027). D. Plane of secondary fluid inclusions in an unbanded center of banded veinlet from Verde East (RV041), showing coexisting type II vapor-rich and type I liquid-rich inclusions.

type II inclusions that have no recognizable liquid. Type IIIa inclusions have negative crystal shapes, 15 to 30 vol percent vapor, and daughter minerals including halite, hematite, and at least two additional unidentified minerals. Measurements of two type IIIa inclusions from an A-veinlet containing magnetite, quartz, and trace chalcopyrite gave halite dissolution temperatures of 625° and 675°C, and salinity estimates of 78 and 84 wt percent NaCl equiv, respectively. The vapor bubbles were still present at 700°C, the upper limit of the heating/freezing stage. The two inclusions are from a single quartz crystal and are not of obvious primary or secondary origin. If these two inclusions formed at the same time, the data suggest that fluids as hot as 675°C circulated through the A-veinlets at Pancho—325ºC higher than the highest temperatures measured from banded quartz veinlets.

Discussion

Occurrence model for the gold deposits at Refugio

The gold deposits at Refugio are hosted by andesitic to dacitic subvolcanic intrusive centers. There is a close spatial and temporal association between gold and stocks of quartz diorite porphyry with microaplitic groundmass and irregular bodies of intrusive breccia. The intrusive rocks were emplaced into coeval volcanics, possibly along fault intersections. The general aspects of a composite volcanic complex can be inferred from the abrupt lateral and vertical facies changes, presence of pumice-poor heterolithic breccias, lack of large-scale ignimbrites, and the presence of composite domes and intrusive breccias (Fig. 3). Based on an arcuate pattern of lava flows along the western and southern edges of the volcanic center, a major vent area, possibly a stratocone, is inferred about a kilometer east of Pancho. Mineralized intrusive centers formed on the flanks of a composite stratovolcano.

Gold mineralization is genetically related to a specific type of quartz veinlet, consisting of banded quartz-magnetite. Because other types of quartz veins are present at Refugio, recognition of veinlet types is crucial in determining the location of highest gold and copper grades. The deepest zone, as exemplified by Pancho, is similar to gold-rich porphyry copper deposits. It is characterized by sugary, irregular quartz veinlets (A-veinlets) in pervasive potassic alteration. The magnetite content approaches 5 vol percent and the total sulfide content is less than 2 vol percent with chalcopyrite as the main sulfide mineral. Zones of A-veinlets without banded quartz veinlets contain the highest hypogene copper grades at

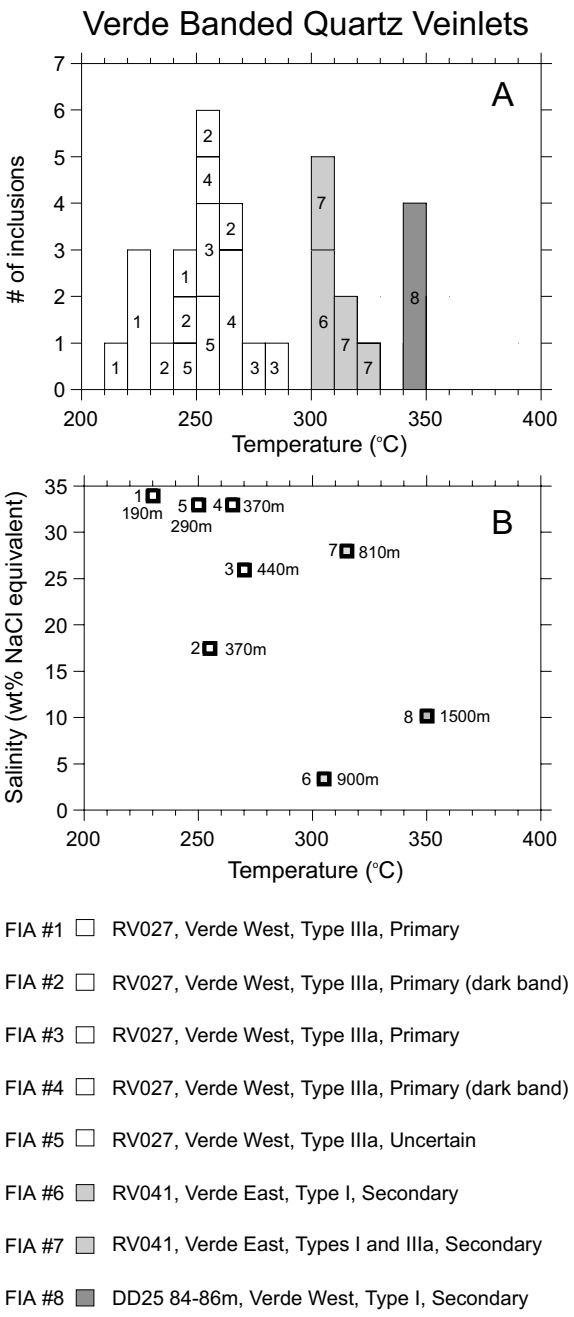

FIG. 16. A. Histogram of liquid-vapor homogenization temperatures of fluid inclusions in banded quartz veinlets from Verde. Numbers refer to fluid inclusion assemblages explained in text. B. Graph of salinity vs. temperature for eight fluid inclusion assemblages, showing hydrostatic depth estimates (see text). NaCl equiv salinities were estimated in type IIIa inclusions by measuring the dissolution temperature of halite and using the equation of Bodnar and Vityk (1994). NaCl equiv salinities of type I inclusions were estimated by measuring the melting temperature of ice and using the equation of Bodnar (1993).

0.1 wt percent and gold grades range from 0.5 to 1 ppm. Thus, ratios of copper to gold (% Cu/ppm Au = ~0.1) in zones of highest copper grade are lower than those in gold-rich porphyry copper deposits (% Cu/ppm Au = 0.39–1.5; Gilmour, 1982; Long, 1995; Sillitoe, 1995; Kirkham and Sinclair, 1996).

The porphyry copperlike environment at Pancho is overlain and locally superimposed by an intermediate zone of banded quartz veinlets that appear to be unique to porphyry gold deposits. At Verde, the zone of banded quartz veinlets constitutes the ore zone and is associated spatially with albitic alteration of plagioclase. The banded veinlets, which lack alteration halos, locally occur in sheeted sets with distinct structural orientations, as seen in the radial-concentric patterns at Verde. Gold occurs paragenetically early in dark bands with micron-sized magnetite and rare copper-iron sulfides and paragenetically late with pyrite and gangue minerals in vuggy vein centers, in fractures that cut the dark bands, and along the vein margins. In zones of abundant banded veinlets without early A-veinlets, gold grades are commonly 1 ppm and copper grades are <0.05 wt percent. Ratios of copper to gold achieve their lowest values (% Cu/ppm Au = ~0.03) in these zones.

Pyritic clay-rich alteration, also containing albite, is peripheral to, overlying, and partially overlapping, the deep and intermediate zones. The pyrite content is only 2 to 4 vol percent, significantly less than in pyritic halos in many porphyry copper deposits. These zones commonly contain quartz-alunite ledges with subeconomic gold grades that locally postdate banded quartz veinlets. Pyritic clay-rich alteration contains ore only where it overprints earlier banded quartz veinlets.

Depths of formation

The depths of formation of the main ore zones in porphyry copper deposits commonly range from 1.5 to 4 km (cf. Sillitoe, 1973; compilation by Muntean, 1998). Based on their geologic setting and fluid inclusion characteristics we estimate that the porphyry gold deposits at Refugio formed at significantly shallower depths.

Using temperatures, salinities, and vapor-saturated conditions described above for fluids forming banded veinlets, we can estimate pressure directly. The steam tables of Haas (1976) for the system NaCl-H_2O, projected from 325° to 350°C, combined with data from eight fluid inclusion assemblages in banded veinlets at Verde, yield pressures in the range from 19 to 150 bars. The local vuggy vein centers and brittle nature of the fractures hosting the banded veinlets suggest that these veinlets formed under hydrostatic pressure. Assuming a density of 1 gm/cm^3 for the overlying column of water, depths below the water table range from 190 to 1,500 m. Depth estimates from pressures for five fluid inclusion assemblages in one sample from Verde West (RV027) are tightly clustered between 190 and 440 m (Fig. 16).

A-veinlets at Pancho yield a minimum temperature of 625°C and a salinity of 80 wt percent NaCl equiv at vapor-saturated conditions. With these data, we calculate a minimum pressure of 250 bars by projecting the results of Bodnar et al. (1985) to the gas plus solid-salt phase boundary where Na and K ratios in liquid are fixed by exchange between albite and K feldspar (Fournier, 1987). Under hydrostatic loads, unlikely given the vein textures, a pressure of 250 bars is equivalent to a depth of 2.5 km, much deeper than that estimated for the banded veinlets. By contrast, under lithostatic pressure, consistent with the textures of A-veinlets, calculated depths are about 1 km, close to estimates for the banded veinlets.

The range in estimated depths based on fluid inclusions could result from fluctuations in the position of the water table and the density of the fluid columns, variations in the amount of volcanic cover due to rapid erosion, and differences between hydrostatic and hydrodynamic pressures (Hedenquist and Henley, 1985). Independent depth estimates, based on stratigraphic reconstructions, suggest that at least 400 to 500 m of rock was removed by erosion above Verde East, and at least 400 m was eroded above the A-veinlets at Pancho (Fig. 3). Regardless of the value chosen, the probable depth range of 0.5 to 1.5 km is significantly shallower than the depths estimated for most porphyry copper deposits.

Origin of garnet veinlets

Previous reports of garnet-bearing veinlets in porphyry-type deposits that lack carbonate host rocks are limited to alkalic porphyry copper deposits (Lang et al., 1995) and high-silica rhyolite porphyry molybdenum deposits (Seedorff, 1988), where the garnet is thought to have formed during cooling of hydrothermal fluids. In contrast, skarn assemblages with andraditic garnets in ejected blocks of hydrothermally altered rock at White Island, New Zealand, have been attributed to heating of a preexisting anhydrite + cristobalite + halite + magnetite assemblage (Wood, 1994). The garnet-bearing veinlets at Verde may have formed in a similar fashion. Fluids at relatively low temperatures in equilibrium with quartz + magnetite + calcite (part of the chlorite-albite-magnetite alteration assemblage) could have been heated by intrusions, leading to the reaction

$$4Fe_3O_4 + 18SiO_2 + 18CaCO_3 + 2H_2O =$$
$$\text{magnetite} + \text{quartz} + \text{calcite} + \text{water} =$$
$$6Ca_2Fe_2Si_3O_{12} + 18CO_2 + 2H_2 . \quad (1)$$
$$\text{andradite} + \text{carbon dioxide} + \text{hydrogen}$$

Reaction (1) indicates that andradite is favored by loss of CO_2 and H_2, consistent with boiling at shallow depths. At oxidation states near the magnetite-hematite buffer, the reaction produces andradite at temperatures above 400° and 350°C at X_{CO_2} = 0.1 and 0.05, respectively (Einaudi, 1982; Bowman, 1998). The absence of garnet-bearing veinlets in porphyry copper deposits could be due to the lack of abundant calcite and iron oxide in the prograding, high-temperature centers of these systems where successive porphyry intrusions are focused. Further, relative to porphyry gold deposits at Refugio, most porphyry copper deposits formed at greater depths. At any given temperature, higher pressure shifts the equilibrium constant for reaction (1) in favor of magnetite-quartz-calcite. Also, decarbonation reactions are likely to be inhibited by the lower permeability of ductile environments at greater depths, which could lead to build-up of carbon dioxide generated by initiation of reaction (1).

Transition from A-veinlets to banded quartz veinlets

The abundance of type II vapor-rich inclusions, the presence of type IIIa inclusions that homogenize by vapor bubble disappearance below 350ºC, and the paucity of type I inclusions have only been reported in a few porphyry copper deposits (i.e., Park Premier; John, 1989). Hypotheses for the origin of banded veinlets need to account not only for the unusual fluid inclusion assemblage, apparently reflecting a relatively rare hydrothermal environment (Figs. 17 and 18), but also the unusual features of texture and mineralogy. Here we discuss our conclusion that banded quartz veinlets resulted from an abrupt transition from lithostatic to hydrostatic pressures at high temperatures. The process shares some aspects of the model first proposed by Gustafson and Hunt (1975) to account for the change in the structure of veins in the El Salvador porphyry copper deposit as this deposit passed through a ductile to brittle transition with time. However, in the porphyry gold deposits at Refugio the fluid evolution and the resulting vein textures and mineralogy were very different because of the contrast in P-T trajectory (Fig. 18).

A-veinlets at Pancho formed from a fluid that was in the three-phase field consisting of a large volume of low-salinity vapor (0.02 wt % NaCl equiv) and much smaller volumes of brine (80 wt % NaCl equiv) and solid salt at 600º to 700ºC and 250 bars lithostatic pressure at a 1-km depth (Fig. 18). At these temperatures, the rock would have been ductile, and fractures could have been open for only short periods of time during periods of high strain rate (Fournier, 1999), consistent with the sugary, granular texture of quartz, the irregular vein walls, and the discontinuous nature of many of the A-veinlets (cf. Gustafson and Hunt, 1975). Direct evidence for a brittle to ductile transition at about 400ºC has been found in active geothermal systems (Fournier, 1991) and is predicted from

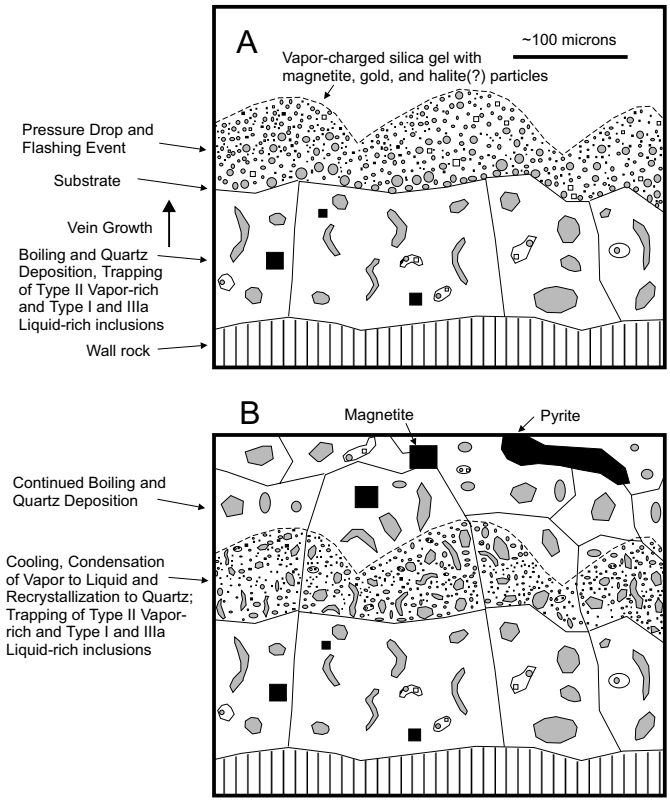

FIG. 17. Schematic diagrams illustrating the formation of banded quartz veinlets. A. Flashing and deposition of vapor-charged silica gel on substrate of earlier quartz. B. Condensation of vapor upon cooling, recrystallization of silica gel to quartz, optically continuous with earlier quartz crystals. Trapping of fluid inclusions. Continued deposition of quartz from boiling fluids.

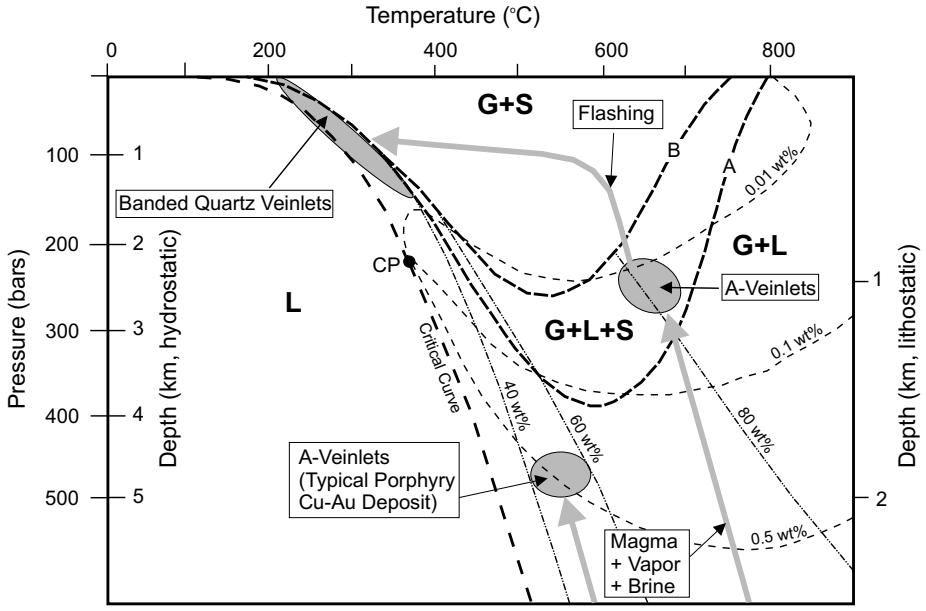

FIG. 18. Phase relationships in the NaCl-H_2O system. Based on the data of Bodnar et al. (1985) and Pitzer and Pabalan(1986; after Fournier, 1987, 1999). CP = critical point for pure H_2O, G = gas, L = liquid, and S = solid salt. Depths assuming a 1 g/cm^3 hydrostatic load and a 2.5 g/cm^3 lithostatic load are also shown. Isopleths of NaCl in liquid and in gas in the two-phase gas + liquid field are shown by the dashed double-dotted lines and short, lightweight dashed lines, respectively. Dashed curve A shows the three-phase boundary, G + L + S, for the system NaCl-H_2O; dashed curve B shows the three-phase boundary, G + L + S for the system NaCl-KCl-H_2O when Na/K ratios are fixed by equilibration with albite and K feldspar at the indicated temperatures. Uncertainties, probably on the order of 100 to 200 bars, are associated with the projections of the isopleths of NaCl in liquid into the three-phase field, G + L + S. The diagram illustrates the flashing of fluids forming A-veinlets during transition from lithostatic to hydrostatic loads and the resulting formation of banded quartz veinlets. Shown for comparison are conditions for formation of A-veinlets in the Far Southeast deposit in the Philippines (Hedenquist et al., 1998) considered to be representative of typical gold-rich porphyry copper deposits.

rock mechanics for wet quartz diorite at about 400ºC and a strain rate of 10^{-14}/sec (Pfiffner and Ramsey, 1982; Fournier, 1999).

In banded quartz veinlets, the continuity of dark bands across parts of individual quartz crystals and the botryoidal texture of the bands are both strong evidence that some of the quartz had a silica gel precursor. According to Weres et al. (1982), if the degree of supersaturation with respect to amorphous silica reaches a factor of about 2.5, homogeneous nucleation is most likely to occur throughout a solution. In this situation, silica polymers grow past critical nucleus size, and colloidal particles become sites for additional silica deposition. The colloidal particles finally coagulate or flocculate, producing gelatinous material. A high degree of supersaturation with respect to amorphous silica can occur as a result of hydrothermal fluid decompression from temperatures above 350ºC (Fournier, 1985).

We propose that dark bands resulted from flashing, due to adiabatic decompression to hydrostatic pressures (cf. King, 1992), of the liquid-vapor mixture that was forming A-veinlets at depth. If the load abruptly changed from lithostatic to hydrostatic at a 1-km depth, the pressure would have dropped from 250 to 100 bars. A fluid at 600º to 700ºC and 100 bars would flash to vapor + salt with very little cooling (Fig. 18), leading to supersaturation with respect to amorphous silica, iron minerals, gold, and halite (Fig. 17A). If sulfur was lost to the vapor phase, precipitation of iron and iron-copper sulfides would have been inhibited, resulting in deposition of magnetite. During flashing the liquid-vapor mixture expanded into zones of lower pressure (cf. Henley and McNabb, 1978). At Pancho, banded quartz veinlets occur at least 125 m above the top of A-veinlets. At Verde, banded quartz veinlets without A-veinlets occur over a vertical interval of at least 500 m.

As the flashing abated, silica colloids coagulated along the fracture walls forming a gel with botryoidal morphology charged with vapor bubbles and micron-sized magnetite, gold, and halite. The continuity of the dark bands at Verde suggests relatively quiescent conditions during formation of the gel. As the gel cooled at constant pressure in the vapor + salt field, it would have intersected the liquid saturation curve in the system H_2O-NaCl at about 300ºC at 100 bars (Fig. 18). At this point droplets and films of water would have condensed from the vapor bubbles. External meteoric water, if present, may have begun to infiltrate the fractures. Given our interpreted pressure-temperature trajectory, halite was present and its subsequent dissolution would have contributed to the wide range of salinities (17–34 wt % NaCl equiv) seen at Verde. Upon cooling the silica gel recrystallized to quartz and trapped any remaining vapor as type II inclusions and any liquid as type I or type IIIa inclusions (Fig. 17B). The fluid inclusions are of primary origin with respect to the quartz but not with respect to silica gel (cf. Sander and Black, 1988) and, therefore, do not record the conditions during flashing and gold-magnetite precipitation.

Although the unbanded parts of the banded veinlets contain the same high ratio of vapor- to liquid-rich inclusions as

the dark bands, they contain less magnetite, fewer vapor-rich inclusions, and no textural evidence of a silica gel precursor. Precipitation within the banded veinlets of the late assemblage of calcite, chlorite, K feldspar, pyrite, with additional gold, suggests the presence of near-neutral pH fluids that may have originated from the loss of acid volatiles, such as HCl, CO_2, and H_2S, during boiling. Condensation of H_2S may have been important in mobilization and redeposition of gold from gold bisulfide complexes in these later stages (cf. Gammons and Willians-Jones, 1997), as possibly indicated by the presence of gold with pyrite in late fractures.

Other deposits with banded quartz veinlets

Banded quartz veinlets are common in the porphyry gold deposits of the Maricunga belt. Based on descriptions in Vila et al. (1991) and King (1992), banded veinlets are the dominant vein type at the Marte deposit (Fig. 2), a deposit with copper:gold ratios similar to those at Verde (Vila et al., 1991). King (1992) suggested that the banded veinlets at Marte formed from a silica gel that resulted from silica supersaturation generated by abrupt pressure decreases, an interpretation supported by the present study. Vila et al. (1991) and King (1992) reported fluid inclusion data from banded veinlets similar to those reported here for Verde, with trapping temperatures below 400ºC (mostly around 250ºC) and salinities up to 40 wt percent NaCl equiv. High-temperature, hypersaline fluid inclusions like those seen in the A-veinlets at Pancho have not been reported from Marte. On the basis of fluid inclusion data and volcanic reconstructions, Vila et al. (1991) estimated that Marte formed at depths of about 500 to 700 m. Outside the Maricunga belt, banded quartz veinlets are reported from El Hueso, Potrerillios district, Chile (Marsh, 1997), Paradise Peak, Nevada (Sillitoe and Lorson, 1994), Zule, California (Canby, 1992), and Palmetto, Nevada (Canby, 1992).

Significance of albite-illite association

Albite with chlorite or illite is the most widespread and characteristic alteration mineral association in the gold deposits at Refugio. Albite-illite alteration appears to be late and occurs at higher structural levels relative to potassic alteration at Pancho and albite-chlorite-magnetite alteration at Verde and may be transitional in time to sericitic alteration. Albite-illite assemblages, with or without calcite, are present in some porphyry copper deposits associated with low potassium granodiorite or tonalitic stocks (e.g., Kabang Kiri, Indonesia: Lowder and Dow, 1978; Park Premier, Utah: John, 1989), as well as at shallow depths in some active geothermal systems hosted by basalt (e.g., Steamboat Springs, Nevada: Sigvaldson and White, 1962; Schoen and White, 1965). At Park Premier, near-surface albitic alteration, accompanied by sericite and/or illite, is interpreted by John (1989) to have resulted from cooling of vapors generated by high-temperature, low-pressure boiling of hypersaline liquids, a model that is supported by experimental studies in the Na-Ca feldspar system (Hemley et al., 1971). This is the model we prefer for albitization at Refugio, in contrast to the heating model in the K-Na feldspar system that causes albitization in the relatively K enriched granodiorites of continental porphyry Cu deposits (e.g., Dilles and Einaudi, 1992).

Conclusions

Both Verde and Pancho are zoned in space from a deeper zone of banded quartz veinlets associated with chlorite-magnetite-albite and/or pyrite-albite-clay alteration to a shallow zone of pyrite-albite-clay and local quartz-alunite ledges. At Verde, the zone of banded quartz veinlets and part of the clay-rich zone are present within the 500 m of vertical exposure available for study. Pancho contains an additional, deepest zone, with A-veinlets and potassic alteration. Relative to Verde, Pancho is telescoped, with all three zones present within a 400-m vertical interval. We have no information on the presence or absence of the zone of A-veinlets at Verde; if A-veinlets are not present at depth below the Verde deposit, then Verde and Pancho evolved differently.

The typical Refugio hydrothermal system (Fig. 19) was initiated with intrusion of quartz diorite porphyry to paleodepths of 1 to 2 km, as seen at Pancho and inferred to be present below Verde. Magmatic-aqueous fluid, both hypersaline liquid and low-salinity vapor, accompanied emplacement of quartz diorite magma and intrusive breccias, presumably from an upper crustal magma chamber. A ductile-brittle boundary at 400ºC was established around the central intrusions. Pressures above the boundary were near hydrostatic, while pressures below the boundary approached lithostatic. Hypersaline liquid, because of its high density, remained in the intrusions below the brittle-ductile boundary at Pancho and led to potassic alteration and copper-gold mineralization (cf. Rye, 1993). As the intrusions cooled at Pancho, fractures remained open for longer periods of time, and A-veinlets became thicker and more continuous. Periodically, upward surges of magma at both deposits breached the ductile-brittle boundary, resulting in explosive pressure release and emplacement of intrusive breccias. At Pancho, these marked the termination of A-veinlet development and the initiation of banded quartz veinlets. At Verde, a reservoir of fluids may not have formed due to the small size of the stocks and the brine flashed without first forming A-veinlets.

Formation of banded quartz veinlets, by flashing of hypersaline liquid, resulted in copper-poor gold mineralization. Radial and concentric fractures at Verde formed during emplacement of late, shallow, weakly mineralized quartz diorite porphyry stocks. Flashed hypersaline liquid traveled upward along the margins of the stocks and into the overlying radial and concentric fractures where it formed banded quartz veinlets. As the stocks continued upward, earlier formed banded quartz veinlets in the host rocks were truncated by the stocks. Rising magmatic vapors enriched in acid volatiles cooled and condensed in near-surface ground water and could have formed the pervasive, shallow pyrite-albite-clay alteration. Where the magmatic vapors were focused along structures, they may have interacted with ground water to form quartz-alunite ledges with slightly anomalous metal values, with a portion of the vapors likely discharging to the surface as fumaroles (e.g., Hedenquist, 1995).

Understanding the causes for variations in the geologic attributes of porphyry-type deposits will continue to improve as research focuses on the differences between deposits. John (1989) proposed that the Park Premier porphyry copper-gold deposit in Utah, a deposit with many similarities to Pancho, is

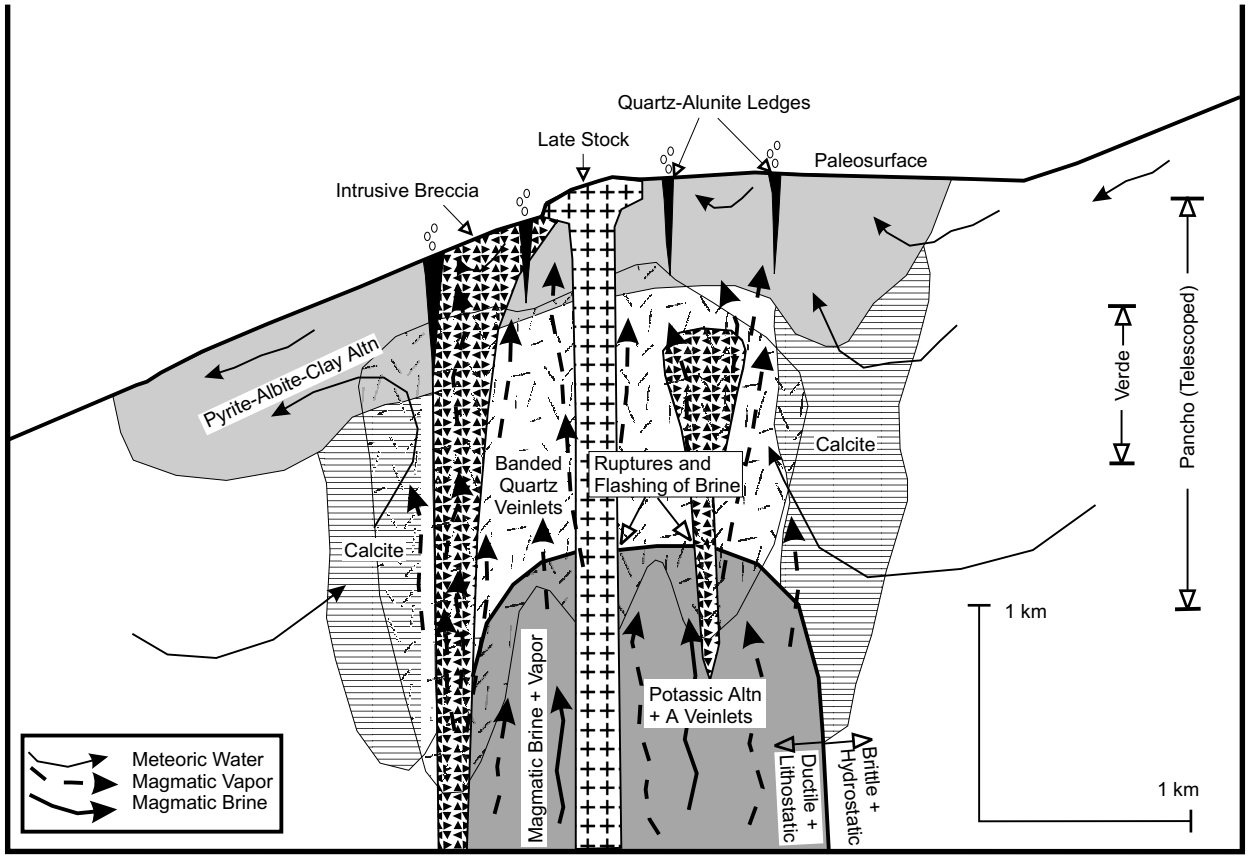

FIG. 19. Schematic cross section showing reconstruction of a typical Refugio hydrothermal system. The figure is time-slice at the peak of intrusive and hydrothermal activity. The quartz diorite stock (labeled "Late Stock" in figure), however, is shown at its final inferred position where it probably reached after the peak of intrusive and hydrothermal activity.

a variation on the theme of porphyry copper deposits brought about by shallow emplacement depths and small sizes of intrusions. A similar argument, taking into account the effect of pressure on the composition of the exsolved magmatic aqueous phase at shallow emplacement depths, was used by Sillitoe (1992) to explain the low copper to gold ratios at Marte. Here, we have stressed another variable that controls the final metal ratios in a porphyry-type deposit: the evolutionary history of the magmatic aqueous phase during its ascent from a source region at unknown depth to the near-surface environment. The key characteristics of porphyry gold deposits, banded quartz veinlets, are the direct result of episodic intrusion of magma and of its associated magmatic aqueous fluids to within 1 km of the surface and the exposure of these high-temperature hydrothermal fluids to hydrostatic pressures. Flashing of the magmatic fluids resulted in the loss of sulfur to vapor during the rupturing events. Since gold and iron do not need sulfur to precipitate, whereas copper does, this loss of sulfur may be the primary cause of the low copper contents of porphyry gold deposits.

Acknowledgments

The authors thank the personnel of Compania Minera Maricunga, Amax Gold, and Bema Gold for funding the field portion and part of the analytical costs of this study. Special thanks go to Neil Muncaster, Albert Brantley, and Roman Flores. We thank Kinross Gold Corporation for allowing this research to be published. A large portion of this research was funded by a National Science Foundation grant EAR9418301 awarded to MTE. We thank Jim Reynolds of Fluid Inc. for numerous discussions on fluid inclusions. Formal reviews by Jeffrey Hedenquist and Werner Halter were very helpful. Additional critical reviews by Richard Sillitoe, David John, John Dilles, and Jim Reynolds are greatly appreciated. Comments by Robert Fournier on hydrothermal phenomena and phase changes related to pressure loss were of great value.

November 8, 1999; May 31, 2000

REFERENCES

Allmendinger, R.W., Figueroa, D., Snyder, D., Beer, J., Mpodozis, C., and Isacks, B.L., 1990, Foreland shortening and crustal balancing in the Andes at 30 degrees S latitude: Tectonics, v. 9, p. 789–809.

Arribas, A., Jr., 1995, Characteristics of high-sulfidation epithermal deposits, and their relation to magmatic fluid: Mineralogical Association of Canada Short Course, v. 23, p. 419–454.

Barazangi, M., and Isacks, B.L., 1976, Spatial distribution of earthquakes and subduction of the Nazca plate beneath South America: Geology, v. 4, p. 686–692.

Bevis, M.G., and Isacks, B.L., 1984, Hypocentral trend surface analysis: Probing the geometry of Benioff zones: Journal of Geophysical Research, v. 89, p. 6153–6170.

Bodnar, R.J., 1993, Revised equation and table for determining the freezing point depression of H_2O-NaCl solutions: Geochimica et Cosmochimica Acta, v. 57, p. 683–684.

Bodnar, R.J., and Vityk, M.O., 1994, Interpretation of microthermometric data for H_2O-NaCl fluid inclusions, *in* De Vivo, B., and Frezotti, M.L., eds. Fluid inclusions in minerals: Methods and application: Blacksburg, VA, Virginia Polytechnic Institute and State University, p. 117–130.

Bodnar, R.J., Burnham, C.W., and Sterner, S.M., 1985, Synthetic fluid inclusions in natural quartz. III. Determination of phase equilibrium properties in the system H_2O-NaCl to 1000°C and 1500 bars: Geochimica et Cosmochimica Acta, v. 49, p. 1871–1873.

Bonatti, E., Harrison, C.G.A., Fisher, D.E., Honnorez, J., Schilling, J.G., and Zentilli, M., 1977, Easter volcanic chain: A mantle hot line: Journal of Geophysical Research, v. 82, p. 2457–2478.

Bowman, J.R., 1998, Basic aspects and applications of phase equilibria in the analysis of metasomatic Ca-Mg-Al-Fe-Si skarns: Mineralogical Association of Canada Short Course Series, v. 26, p. 1–50.

Boydell, H.C., 1924, The role of colloidal solutions in the formation of mineral deposits: Institution of Mining and Metallurgy Transactions, v. 34, p. 145–337.

Brown, A.J., and Rayment, B., 1991, Refugio gold project, Chile: Mining Magazine, November issue, p. 306–312.

Canby, V.M., 1992, Porphyry-type gold mineralization of late Neogene age at the Zule volcanic center, Sierra County, California: Unpublished M.Sc. thesis, Reno, University of Nevada, 109 p.

Carten, R.B., 1987, Sodium-calcium metasomatism: Chemical, temporal, and spatial relationships at the Yerington, Nevada, porphyry copper deposit: Economic Geology, v. 81, p. 1495–1519.

Cox, D.P., 1985, Geology of the Tanama and Helecho porphyry copper deposits and vicinity, Puerto Rico: U.S. Geological Survey Professional Paper 1327, 57 p.

Davidson, J., and Mpodozis, C., 1991, Regional geologic setting of epithermal gold deposits, Chile: Economic Geology, v. 86, p. 1174–1186.

Dilles, J.H., and Einaudi, M.T., 1992, Wall-rock alteration and hydrothermal flow paths about the Ann-Mason porphyry copper deposit, Nevada: A 6-km vertical reconstruction: Economic Geology, v. 87, p. 1963–2001.

Einaudi, M.T., 1982, General features and origin of skarns associated with porphyry copper plutons—southwestern North America, *in* Titley, S.R., ed., Advances in geology of the porphyry copper deposits, southwestern North America: Tucson, University of Arizona Press, p. 185–210.

Flores, R., 1993, Geologia del porfido aurifero Verde, proyecto Refugio, Tercera region, Chile: Revista Geologica de Chile, v. 20, p. 57–69.

Fournier, R.O., 1985, The behavior of silica in hydrothermal solutions: Reviews in Economic Geology, v. 2, p. 45–60.

——1987, Conceptual models of brine evolution: U.S. Geological Survey Professional Paper 1350, v. 2, p. 1487–1506.

——1991, The transition from hydrostatic to greater than hydrostatic fluid pressure in presently active continental hydrothermal systems in crystalline rock: Geophysical Research Letters, v. 18, p. 955–958.

——1999, Hydrothermal processes related to movement of fluid from plastic into brittle rock in the magmatic-epithermal environment: Economic Geology, v. 94, p. 1193–1211.

Gammons, C.H., and Williams-Jones, A.E., 1997, Chemical mobility of gold in the porphyry-epithermal environment: Economic Geology, v. 92, p. 45–59.

Gilmour, P., 1982, Grades and tonnages of porphyry copper deposits, *in* Titley, S.R., ed., Advances in geology of the porphyry copper deposits, southwestern North America: Tucson, University of Arizona Press, p. 7–35.

Goldstein, R.H., and Reynolds, T.J., 1994, Systematics of fluid inclusions in diagenetic minerals: Society of Economic Paleontologists and Mineralogists Short Course 31, 199 p.

Gustafson, L.B., 1978, Some major factors of porphyry copper genesis: Economic Geology, v. 73, p. 600–607.

Gustafson, L.B., and Hunt, J.P., 1975, The porphyry copper deposit at El Salvador, Chile: Economic Geology, v. 70, p. 857–912.

Haas, J.L., Jr., 1976, Physical properties of the coexisting phases and thermochemical properties of the H_2O component of boiling NaCl solutions: U.S. Geological Survey Bulletin 1421-A, 73 p.

Hedenquist, J.W., 1995, The ascent of magmatic fluid: Discharge versus mineralization: Mineralogical Association of Canada Short Course, v. 23, p. 263–289.

Hedenquist, J.W., and Henley R.W., 1985, Hydrothermal eruptions in the Waiotapu geothermal system, New Zealand: Their origin, associated breccias, and relation to precious metal mineralization: Economic Geology, v. 80, p. 1640–1668.

Hedenquist, J.W., Arribas, A., Jr., and Reynolds, T.J., 1998, Evolution of an intrusion-centered hydrothermal system: Far Southeast-Lepanto porphyry and epithermal Cu-Au deposits, Philippines: Economic Geology, v. 93, p. 373–404.

Hemley, J.J., Hostetler, P.B., Gude, A.J., and Mountjoy, W.T., 1969, Some stability relations of alunite: Economic Geology, v. 64, p. 599–612.

Hemley, J.J., Montoya, J.W., Nigrini, A., and Vincent, H.A., 1971, Some alteration reactions in the system CaO-Al_2O_3-SiO_2-H_2O: Society of Mining Geologists of Japan Special Issue 2, p. 58–63.

Hemley, J.J., Montoya, J.W., Marinenko, J.W., and Luce, R.W., 1980, Equilibria in the system Al_2O_3-SiO_2-H_2O and some general implications for alteration-mineralization processes: Economic Geology, v. 75, p. 210–228.

Henley, R.W., and McNabb, A., 1978, Magmatic vapor plumes and groundwater interaction in porphyry copper emplacement: Economic Geology, v. 73, p. 1–20.

Isacks, B.L., 1988, Uplift of the central Andean plateau and bending of the Bolivian orocline: Journal of Geophysical Research, v. 93, p. 3211–3231.

John, D.A., 1989, Evolution of hydrothermal fluids in the Park Premier stock, central Wasatch Mountains, Utah: Economic Geology, v. 84, p. 879–902.

Jordan, T.E., Isacks, B.L., Allmendinger, R.W., Brewer, J.A., Ramos, V.A., and Ando, C.J., 1983, Andean tectonics related to geometry of subducted Nazca plate: Geological Society of America Bulletin, v. 94, p. 341–361.

Kay, S.M., Mpodozis, C., Ramos, V.A., and Munizaga, F., 1991, Magma source variations for mid-late Tertiary magmatic rocks associated with a shallowing subduction zone and a thickening crust in the central Andes (28 to 33°S): Geological Society of America Special Paper 265, p. 113–137.

Kay, S.M., Mpodozis, C., Tittler, A., and Cornejo, P., 1994, Tertiary magmatic evolution of the Maricunga mineral belt in Chile: International Geology Reviews, v. 36, p. 1079–1112.

Kesler, S.E., 1973, Copper, molybdenum, and gold abundances in porphyry copper deposits: Economic Geology, v. 68, p. 106–112.

King, A.R., 1992, Magmatism, structure and mineralization in the Maricunga belt, N. Chile: Unpublished Ph.D. thesis, London, U.K., Imperial College, 395 p.

Kirkham, R.V., and Sinclair, W.D., 1996, Porphyry copper, gold, molybdenum, tungsten, tin, silver: Geological Survey of Canada, Geology of Canada, no. 8, p. 421–446.

Lang, J.R., Stanley, C.R., Thompson, J.F.H., and Dunne, K.P.E., 1995, Na-K-Ca magmatic-hydrothermal alteration in alkalic porphyry Cu-Au deposits, British Columbia: Mineralogical Association of Canada Short Course, v. 23, p. 339–366.

Long, K.R., 1995, Production and reserves of Cordilleran (Alaska to Chile) porphyry copper deposits: Arizona Geological Society Digest, v. 20, p. 316–335.

Lowder, G.C., and Dow, J.A.S., 1978, Geology and exploration of porphyry copper deposits in north Sulawesi, Indonesia: Economic Geology, v. 73, p. 628–644.

Lowell, J.D., and Guilbert, J.M., 1970, Lateral and vertical alteration-mineralization zoning in porphyry ore deposits: Economic Geology, v. 65, p. 373–408.

Marsh, T.M., 1997, Geochronology, thermochronology, and stable isotope systematics of the Cu-Au and Au-Ag deposits of the Potrerillos district, Atacama region, Chile: Unpublished Ph.D. thesis, Stanford, CA, Stanford University, 411 p.

McKee, E.H., Robinson, A.C., Rytuba, J.J., Cuttino, L., and Moscoso, R.D., 1994, Age and Sr isotopic composition of volcanic rocks in the Maricunga belt, Chile: Implications for magma sources: Journal of South American Earth Sciences, v. 7, p. 167–177.

Mercado W., M., 1982, Geologia de la Hoja Laguna del Negro Francisco, Region de Atacama: Santiago, Servicio Nacional Geologia Mineria, Carta Geologica, Chile, no. 56, 73 p.

Mpodozis, C., Cornejo, P., Kay, S.M., and Tittler, A., 1995, La Franja de Maricunga: sintesis de la evolucion del Frente Volcanico Oligoceno-Mioceno de la zona sur de los Andes Centrales: Revista Geologica de Chile, v. 21, p. 273–313.

Muntean, J.L., 1998, Magmatic-hydrothermal gold deposits of the Maricunga belt, northern Chile: Unpublished Ph.D. thesis, Stanford, CA, Stanford University, 400 p.

Nash, J.T., 1976, Fluid-inclusion petrology—data from porphyry copper deposits and applications to exploration: U.S. Geological Survey Professional Paper 907D, 16 p.

Oviedo, L., Fuster, N., Tschischow, N., Ribba, L., Zuccone, A., Grez, E., and Aguilar, A., 1991, General geology of the La Coipa precious metal deposit, Atacama, Chile: Economic Geology, v. 86, p. 1287–1300.

Pfiffner, O.A., and Ramsay, J.G., 1982, Constraints on geological strain rates: Arguments from finite strain rates of naturally deformed rocks: Journal of Geophysical Research, v. 87, p. 311–321.
Pitzer, K.S., and Pabalan, R.T., 1986, Thermodynamics of NaCl in steam: Geochimica et Cosmochimica Acta, v. 50, p. 1445–1454.
Ramdohr, P., 1980, The ore minerals and their intergrowths, 2nd. ed.: New York, Permagon, 1207 p.
Ramos, V.A., Jordan, T.E., Allmendinger, R.W., Mpodozis, C., Kay, S.M., Cortes, J.M., and Palma, M., 1986, Paleozoic terranes of the Central Argentine-Chilean Andes: Tectonics, v. 5, p. 855–886.
Rodriguez, M., Osvaldo, R., Branko, R., Carrasco, M., and Romero I., 1997, Caracterizacion geoquimica de granates del yaciemiento Verde, distrito Refugio, III Region, Chile: Congreso Geologica Chileno, 8th, Actas, Antofagasta.
Rye, R.O., 1993, The evolution of magmatic fluids in the epithermal environment: The stable isotope perspective: ECONOMIC GEOLOGY, v. 88, p. 733–752.
Rye, R.O., Bethke, P.M., and Wasserman, M.D., 1992, The stable isotope geochemistry of acid-sulfate alteration: ECONOMIC GEOLOGY, v. 87, p. 225–262.
Sander, M.V., and Black, J.E., 1988, Crystallization and recrystallization of growth-zoned vein quartz crystals from epithermal systems: Implications for fluid inclusion studies: ECONOMIC GEOLOGY, v. 83, p. 1052–1060.
Sasso, A.M., and Clark, A.H., 1998, The Farallon Negro Group, northwest Argentina: Magmatic, hydrothermal and tectonic evolution and implications for Cu-Au metallogeny in the Andean back-arc: Society of Economic Geologists Newsletter, no. 34, p. 1–18.
Schoen, R., and White, D.E., 1965, Hydrothermal alteration in GS-3 and GS-4 drill holes, Main terrace, Steamboat Springs, Nevada: ECONOMIC GEOLOGY, v. 60, p. 1411–1421.
Seedorff, E., 1988, Cyclic development of hydrothermal mineral assemblages related to multiple intrusions at the Henderson porphyry molybdenum deposit, Colorado: Canadian Institute for Mining and Metallurgy Special Volume 39, p. 367–393.
Segerstrom, K., 1968, Geologia de las Hojas Copiapo y Ojos del Salada, Provincia de Atacama: Santiago, Chile, Instituto de Investigaciones Geológicas Boletín 24, 58 p.
Sigvaldson, G.E., and White, D.E., 1962, Hydrothermal alteration in drill holes GS-5 and GS-7, Steamboat Springs, Nevada: U.S. Geological Survey Professional Paper 450-D, p. D113–D117.
Sillitoe, R.H., 1973, The tops and bottoms of porphyry copper deposits: ECONOMIC GEOLOGY, v. 68, p. 799–815.
——1979, Some thoughts on gold-rich porphyry copper deposits: Mineralium Deposita, v. 14, p. 161–174.
——1992, Gold and copper metallogeny of the central Andes: Past, present, and future exploration objectives: ECONOMIC GEOLOGY, v. 87, p. 2205–2216.
——1993, Gold-rich porphyry copper deposits: Geological model and exploration implications: Geological Association of Canada Special Paper 40, p. 465–478.
——1995, Exploration and discovery of base- and precious-metal deposits in the Circum-Pacific region during the last 25 years: Resource Geology Special Issue 19, 119 p.
Sillitoe, R.H., and Lorson, R.C., 1994, Epithermal gold-silver-mercury deposits at Paradise Peak, Nevada: Ore controls, porphyry gold association, detachment faulting, and supergene oxidation: ECONOMIC GEOLOGY, v. 89, p. 1228–1248.
Sillitoe, R.H., McKee, E.H., and Vila, T., 1991, Reconnaissance K-Ar geochronology of the Maricunga gold-silver belt, northern Chile: ECONOMIC GEOLOGY, v. 86, p. 1261–1270.
Titley, S.R., ed., 1966, Geology of the porphyry copper deposits, southwestern North America: Tucson, University of Arizona Press, 287 p.
Titley, S.R., and Beane, R.E., 1981, Porphyry copper deposits: Part I. Geologic settings, petrology, and tectogenesis: ECONOMIC GEOLOGY SEVENTY-FIFTH ANNIVERSARY VOLUME, p. 214–234.
Tosdal, R.M., 1996, The Amazon-Laurentian connection as viewed from the Middle Proterozoic rocks in the central Andes, western Bolivia and northern Chile: Tectonics, v. 15, p. 827–842.
Vila, T., and Sillitoe, R.H., 1991, Gold-rich porphyry systems in the Maricunga belt, northern Chile: ECONOMIC GEOLOGY, v. 86, p. 1238–1260.
Vila, T., Sillitoe, R.H., Betzhold, J., and Viteri, E., 1991, The porphyry gold deposit at Marte, northern Chile: ECONOMIC GEOLOGY, v. 86, p. 1271–1286.
Walker, J.A., Moulds, T.N., Zentilli, M., and Feigenson, M.D., 1991, Spatial and temporal variations in volcanics of the Andean central volcanic zone (26 to 28°S): Geological Society of America Special Paper 265, p. 139–155.
Weres, O., Yee, A., and Tsao, L., 1982, Equations and type curves for predicting the polymerization of amorphous silica in geothermal brines: Society of Petrological Engineering Journal, February 1982, p. 9–16.
Wood, C.P., 1994, Mineralogy at the magma-hydrothermal system interface in andesite volcanoes: Geology, v. 22, p. 75–78.
Zentilli, M., 1974, Geological evolution and metallogenic relationships in the Andes of northern Chile between 26° and 29° South: Unpublished Ph.D. thesis, Kingston, ON, Canada, Queen's University, 446 p.